Computer Physics Communications 252 (2020) 106773

Contents lists available at ScienceDirect

Computer Physics Communications

journal homepage: www.elsevier.com/locate/cpc

HALO: A full-orbit model of nonlinear interaction of fast particles with eigenmodes

M. Fitzgerald [a,*], J. Buchanan [a], R.J. Akers [a], B.N. Breizman [b], S.E. Sharapov [a]

[a] CCFE, Culham Science Centre, Abingdon, Oxon, OX14 3DB, United Kingdom
[b] Institute for Fusion Studies, The University of Texas at Austin, Austin, TX 78712, United States of America

ARTICLE INFO

Article history:
Received 15 February 2019
Accepted 8 April 2019
Available online 28 April 2019

Keywords:
Fast
Particle
Plasma
Eigenmode
Wave
Alfvén
Nonlinear
TAE

ABSTRACT

HALO (HAgis LOcust) solves the initial value Vlasov–Maxwell problem perturbatively for application to certain nonlinear wave-particle problems in tokamak plasmas. It uses the same basic approach as the HAGIS code (Pinches et al., 1998) for wave evolution but is built on the LOCUST-GPU full-orbit code (Akers et al., 2012) for the solution of the Hamiltonian fast particle motion in cylindrical coordinates. The wave amplitude and particle evolution include all finite Larmor radius effects. We describe and benchmark the currently implemented Alfvén eigenmode workflow, demonstrating correct particle motion, linear and nonlinear power transfer. The formulation and numerical scheme are sufficiently general as to allow easy future implementation of different kinds of eigenmodes, such as modes close to the ion-cyclotron frequency. The code can model multiple eigenmodes and multiple fast ion species simultaneously, and supports the general form of the equilibrium distribution in constants of motion.

1. Introduction

For tokamaks to allow reactor relevant regimes of operation, a proportion of the confined plasma must necessarily be comprised of energetic ions. The anticipated abundance of non-Maxwellian alpha particles in the burning plasma regime on ITER would be both a key physics achievement and a new stability consideration. It is well understood, both from current experiments and significant theoretical study, that fast particles can resonantly destabilize wave eigenmodes in the bulk thermonuclear tokamak plasma, which can degrade performance and damage the plasma-facing components through energetic ion redistribution and loss.

Existing experiments with neutral beam injection (NBI) and ion cyclotron resonant heating (ICRH) have confirmed the destabilization of predicted bulk plasma eigenmodes such as the toroidal Alfvén eigenmode (TAE) [1] or the reverse shear Alfvén eigenmode (RSAE) [2]. In addition to the well-understood Alfvénic modes in the bulk plasma, wave activity in the ion-cyclotron range has also been observed, as well as lower frequency energetic particle modes (EPM) [3] which are thought to be large coherent motions of the fast-particles themselves interacting with a broad Alfvén continuum. A number of stability modelling strategies have been employed with varying levels of self-consistency and difficulty [4].

For the Alfvénic modes that have been identified as eigenmodes of the bulk plasma, very good agreement has been shown between the linear MHD theory and the observations [5]. This experimental fact is a powerful motivation for a general perturbative nonlinear predictive code for wave-particle interaction, where all the nonlinearity is assumed to be due to the perturbed fast ions rather than the bulk plasma. The perturbative approach is fundamentally the same as the nonlinear Landau damping solution given by O'Neil [6] and Mazitov [7] and later applied to Alfvén waves in the fusion context by Berk and Breizman [8], where particle orbits in tokamak geometry were computed using a guiding centre drift model with a simplified Alfvén wave expression [9]. The formulation of a Hamiltonian theory of guiding centre motion in realistic magnetic geometry [10] allowed similar solutions of the drift-kinetic-Maxwell problem in codes such as ORBIT [11], FAC [12] and HAGIS [13]. All these codes relied on a delta-f scheme [14], forcing the identically zero equilibrium contribution to the power transfer to be ignored in the marker population, improving Monte Carlo statistics in the remaining contribution coming from the perturbation.

In this work, we present the new HALO (HAgis LOcust) code, which is a full orbit implementation of the perturbative delta-f approach, allowing nonlinear modelling of any bulk plasma eigenmode at arbitrary frequency using the Vlasov–Maxwell system of equations. The high performance LOCUST-GPU code [15] serves as the orbit following foundation for the wave-particle physics described in this paper.

* Corresponding author.
E-mail address: Michael.Fitzgerald@ukaea.uk (M. Fitzgerald).

https://doi.org/10.1016/j.cpc.2019.04.006

2. Physical model

In this section, we rederive a perturbative wave-particle treatment for a general Vlasov–Maxwell system and an associated delta-f noise reduction scheme. Our goal is to make the derivation sufficiently general to be useful to those working in both astrophysical and laboratory plasmas, as well as to make the orderings required for the perturbative approach as transparent as possible. We deviate from the usual variational approach [9] and instead start with Maxwell's equations.

2.1. Derivation of wave evolution equations

Starting with the Fourier transformed wave-equation

$$-\frac{c^2}{\omega^2}\nabla\times\nabla\times\tilde{\mathbf{E}}(\boldsymbol{x},\omega)+\tilde{\mathbf{E}}(\boldsymbol{x},\omega)=-\frac{i\mu_0c^2}{\omega}\tilde{\mathbf{J}}(\boldsymbol{x},\omega) \tag{1}$$

we may identify the linear response of the total current density, and separate it from the nonlinear $\tilde{\mathbf{J}}_{\boldsymbol{NL}}(\boldsymbol{x},\omega)$ and free current $\tilde{\mathbf{J}}_{free}(\boldsymbol{x},\omega)$

$$\begin{aligned}&-\frac{c^2}{\omega^2}\nabla\times\nabla\times\tilde{\mathbf{E}}(\boldsymbol{x},\omega)+\tilde{\mathbf{E}}(\boldsymbol{x},\omega)\\&=-\frac{i\mu_0c^2}{\omega}\left[\int d\boldsymbol{x}'\boldsymbol{\sigma}\left(\boldsymbol{x},\boldsymbol{x}',\omega\right)\tilde{\mathbf{E}}\left(\boldsymbol{x}',\omega\right)+\tilde{\mathbf{J}}_{\boldsymbol{NL}}(\boldsymbol{x},\omega)\right.\\&\left.+\tilde{\mathbf{J}}_{free}(\boldsymbol{x},\omega)+\tilde{\mathbf{J}}_{\bar{\sigma}}(\boldsymbol{x},\omega)\right]\end{aligned} \tag{2}$$

This rearrangement has been expressed a number of equivalent ways in the literature [16,17] such as

$$K\left(\boldsymbol{x},\boldsymbol{x}',\omega\right)=\frac{\boldsymbol{\epsilon}\left(\boldsymbol{x},\boldsymbol{x}',\omega\right)}{\epsilon_0}=\left(\delta\left(\boldsymbol{x}-\boldsymbol{x}'\right)\mathbf{I}+\frac{i\mu_0c^2}{\omega}\boldsymbol{\sigma}\left(\boldsymbol{x},\boldsymbol{x}',\omega\right)\right) \tag{3}$$

$$\Lambda\left(\boldsymbol{x},\boldsymbol{x}',\omega\right)=\left[-\frac{c^2}{\omega^2}\delta\left(\boldsymbol{x}-\boldsymbol{x}'\right)\nabla'\times\nabla'\times+K\left(\boldsymbol{x},\boldsymbol{x}',\omega\right)\right] \tag{4}$$

where $K\left(\boldsymbol{x},\boldsymbol{x}',\omega\right)$ is the dimensionless dielectric tensor and the corresponding wave equation is

$$\begin{aligned}&\int d\boldsymbol{x}'\Lambda\left(\boldsymbol{x},\boldsymbol{x}',\omega\right)\tilde{\mathbf{E}}(\boldsymbol{x}',\omega)\\&=-\frac{i\mu_0c^2}{\omega}\left(\tilde{\mathbf{J}}_{\boldsymbol{NL}}(\boldsymbol{x},\omega)+\tilde{\mathbf{J}}_{free}(\boldsymbol{x},\omega)+\tilde{\mathbf{J}}_{\bar{\sigma}}(\boldsymbol{x},\omega)\right)\end{aligned} \tag{5}$$

Without loss of generality, we can require that the conductivity $\boldsymbol{\sigma}\left(\boldsymbol{x},\boldsymbol{x}',\omega\right)$ is chosen in such a way as to keep the dielectric tensor $K\left(\boldsymbol{x},\boldsymbol{x}',\omega\right)$ equal to the transpose of its complex conjugate

$$K\left(\boldsymbol{x},\boldsymbol{x}',\omega\right)=K^{\dagger}\left(\boldsymbol{x},\boldsymbol{x}',\omega\right) \tag{6}$$

and express remaining linear currents by the $\tilde{\mathbf{J}}_{\bar{\sigma}}(\boldsymbol{x},\omega)$ term. It is well known that if the dielectric tensor has this Hermitian matrix property then solutions to the wave equation in the absence of other currents conserve energy. Moreover, under appropriate boundary conditions the differential wave operator is self-adjoint under the inner product

$$\begin{aligned}&\int d\boldsymbol{x}\int d\boldsymbol{x}'\ \mathbf{a}^{\dagger}(\boldsymbol{x})\Lambda\left(\boldsymbol{x},\boldsymbol{x}',\omega\right)\mathbf{b}(\boldsymbol{x}')\\&=\int d\boldsymbol{x}\int d\boldsymbol{x}'\ \mathbf{b}^{\dagger}(\boldsymbol{x})\Lambda\left(\boldsymbol{x},\boldsymbol{x}',\omega\right)\mathbf{a}(\boldsymbol{x}')\end{aligned} \tag{7}$$

We will adopt the notation of Breizman et al. [18] making all terms in the wave equation have dimensions of current density

$$g\left(\boldsymbol{x},\boldsymbol{x}',\omega\right)\equiv-\frac{\omega}{i\mu_0c^2}\Lambda\left(\boldsymbol{x},\boldsymbol{x}',\omega\right) \tag{8}$$

$$\int d\boldsymbol{x}'\ g\left(\boldsymbol{x},\boldsymbol{x}',\omega\right)\tilde{\mathbf{E}}(\boldsymbol{x}',\omega)=\tilde{\mathbf{J}}_{\boldsymbol{NL}}(\boldsymbol{x},\omega)+\tilde{\mathbf{J}}_{free}(\boldsymbol{x},\omega)+\tilde{\mathbf{J}}_{\bar{\sigma}}(\boldsymbol{x},\omega) \tag{9}$$

Consider the linear homogeneous (undriven) MHD equation

$$\int d\boldsymbol{x}'\ \mathrm{g}_{\mathrm{MHD}}\left(\boldsymbol{x},\boldsymbol{x}',\omega\right)\tilde{\mathbf{E}}(\boldsymbol{x}',\omega)=0 \tag{10}$$

This formalism supports any model for the plasma conductivity $\boldsymbol{\sigma}\left(\boldsymbol{x},\boldsymbol{x}',\omega\right)$ that makes the dielectric $K\left(\boldsymbol{x},\boldsymbol{x}',\omega\right)$ Hermitian, so it is not restricted to just linear MHD. However, given the examples in this paper deal with shear Alfvén waves, we will label the linear response with "MHD" for the purposes of this derivation, but we will drop the label outside this derivation in order to avoid the implication that it *has* to be MHD.

The corresponding inhomogeneous (driven) MHD problem is

$$\int d\boldsymbol{x}'\ \mathrm{g}_{\mathrm{MHD}}\left(\boldsymbol{x},\boldsymbol{x}',\omega\right)\tilde{\mathbf{E}}(\boldsymbol{x}',\omega)=\tilde{\mathbf{J}}_{free}(\mathbf{x},\omega) \tag{11}$$

The free currents are independent of the electric field (by definition). If the drive from free currents is sufficiently weak, then solutions to an externally driven inhomogeneous equation at ω near ω' will resemble a homogeneous solution at ω'. We thus assume $|\omega|\gg|\omega-\omega'|$

$$\begin{aligned}\mathrm{g}_{\mathrm{MHD}}\left(\boldsymbol{x},\boldsymbol{x}',\omega\right)\approx\mathrm{g}_{\mathrm{MHD}}\left(\boldsymbol{x},\boldsymbol{x}',\omega'\right)+\epsilon\left[\left(\omega-\omega'\right)\frac{\partial}{\partial\omega}\right]\\\cdot\mathrm{g}_{\mathrm{MHD}}\left(\boldsymbol{x},\boldsymbol{x}',\omega'\right)\end{aligned} \tag{12}$$

where we have introduced the formal small ordering parameter ϵ which is the ratio of driving current to the dielectric currents

$$\frac{\left|\omega-\omega'\right|}{|\omega|}\sim\frac{\left|\tilde{\mathbf{J}}_{free}(\boldsymbol{x},\omega)\right|}{\left|\int d\boldsymbol{x}'\ \sigma_{\mathrm{MHD}}\left(\boldsymbol{x},\boldsymbol{x}',\omega\right)\tilde{\mathbf{E}}(\boldsymbol{x}',\omega)\right|}\ll1 \tag{13}$$

We include ϵ simply as a label to remind the relative sizes of various terms, which should be set $\epsilon=1$ to obtain the physical formulas.

The weakly driven MHD problem becomes

$$\begin{aligned}&\int d\boldsymbol{x}'\left[\mathrm{g}_{\mathrm{MHD}}\left(\boldsymbol{x},\boldsymbol{x}',\omega'\right)+\epsilon\left[\left(\omega-\omega'\right)\frac{\partial\mathrm{g}_{\mathrm{MHD}}\left(\boldsymbol{x},\boldsymbol{x}',\omega'\right)}{\partial\omega}\right]\right]\\&\cdot\tilde{\mathbf{E}}\left(\boldsymbol{x}',\omega\right)\\&=\epsilon\tilde{\mathbf{J}}_{free}(\boldsymbol{x},\omega)\end{aligned} \tag{14}$$

The weakly driven MHD problem outlined above is analogous to certain classes of wave-particle problems where the currents are not free. In these problems, the plasma response currents are dominated by linear Hermitian dielectric currents, and the remaining nonlinear and linear response currents are deemed much smaller in comparison

$$\begin{aligned}&\int d\boldsymbol{x}'\left[\mathrm{g}_{\mathrm{MHD}}\left(\boldsymbol{x},\boldsymbol{x}',\omega'\right)+\epsilon\left[\left(\omega-\omega'\right)\frac{\partial}{\partial\omega}\right]\mathrm{g}_{\mathrm{MHD}}\left(\boldsymbol{x},\boldsymbol{x}',\omega'\right)\right]\\&\cdot\tilde{\mathbf{E}}\left(\boldsymbol{x}',\omega\right)\\&=\epsilon\tilde{\mathbf{J}}_{\boldsymbol{NL}}(\boldsymbol{x},\omega)+\epsilon\tilde{\mathbf{J}}_{\bar{\sigma}}(\boldsymbol{x},\omega)\end{aligned} \tag{15}$$

$$\begin{aligned}\frac{\left|\omega-\omega'\right|}{|\omega|}&\sim\frac{\left|\tilde{\mathbf{J}}_{\bar{\sigma}}(\boldsymbol{x},\omega)\right|}{\left|\int d\boldsymbol{x}'\ \sigma_{\mathrm{MHD}}\left(\boldsymbol{x},\boldsymbol{x}',\omega\right)\tilde{\mathbf{E}}(\boldsymbol{x}',\omega)\right|}\\&\sim\frac{\left|\tilde{\mathbf{J}}_{\boldsymbol{NL}}(\boldsymbol{x},\omega)\right|}{\left|\int d\boldsymbol{x}'\ \sigma_{\mathrm{MHD}}\left(\boldsymbol{x},\boldsymbol{x}',\omega\right)\tilde{\mathbf{E}}(\boldsymbol{x}',\omega)\right|}\ll1\end{aligned} \tag{16}$$

These orderings must be motivated by the specific wave phenomena being studied (see Appendix for TAE discussion). The weak

current sources depend on the electric field, so to form a closed system for the electric field, the relationship between the current sources and the electric field must be known.

We now seek to solve the wave equation for the nonlinear interaction of resonant and non-resonant fast particles. We combine the source currents into one term $\tilde{\mathbf{J}}_{\boldsymbol{fast}}(\mathbf{x},\omega)$

$$\int d\boldsymbol{x}'\left[\mathrm{g}_{\mathrm{MHD}}\left(\boldsymbol{x},\boldsymbol{x}',\omega'\right)+\epsilon\left[\left(\omega-\omega'\right)\frac{\partial}{\partial\omega}\right]\mathrm{g}_{\mathrm{MHD}}\left(\boldsymbol{x},\boldsymbol{x}',\omega'\right)\right]\cdot\tilde{\mathbf{E}}\left(\boldsymbol{x}',\omega\right)=\epsilon\tilde{\mathbf{J}}_{\boldsymbol{fast}}\left(\boldsymbol{x},\omega\right)\tag{17}$$

Note the subtle difference between demanding that the fast particle contribution be small and the weaker assumption that the resonant and nonlinear contribution be small. It is well known that MHD is not sufficient to describe the Hermitian dielectric motion of fast particles, since particles can drift from flux surfaces. Care must be taken not to double count Hermitian dielectric current contributions in any choice of bulk plasma model. This so-called 'adiabatic' contribution is discussed in the Appendix.

Exploiting the property that $\Lambda\left(\boldsymbol{x},\boldsymbol{x}',\omega\right)$ is self-adjoint with electric field eigenmodes $\boldsymbol{e}\left(\boldsymbol{x},\omega';\omega_j\right)$, we may multiply by any adjoint eigenmode $\boldsymbol{e}^{\dagger}\left(\boldsymbol{x},\omega';\omega_j\right)$

$$\int d\boldsymbol{x}\int d\boldsymbol{x}'\;\boldsymbol{e}^{\dagger}\left(\boldsymbol{x};\omega_j\right)\delta\left(\omega'-\omega_j\right)\left[\left(\omega-\omega'\right)\frac{\partial}{\partial\omega}\right]\cdot\mathrm{g}_{\mathrm{MHD}}\left(\boldsymbol{x},\boldsymbol{x}',\omega'\right)\tilde{\mathbf{E}}\left(\boldsymbol{x}',\omega\right)=\delta\left(\omega'-\omega_j\right)\int d\boldsymbol{x}\;\boldsymbol{e}^{\dagger}\left(\boldsymbol{x};\omega_j\right)\tilde{\mathbf{J}}_{\boldsymbol{fast}}\left(\boldsymbol{x},\omega\right)\tag{18}$$

Integrating and performing the inverse transform to reobtain the real field $\delta\boldsymbol{E}\left(\boldsymbol{x}',t\right)$

$$\int d\boldsymbol{x}\int d\boldsymbol{x}'\;\boldsymbol{e}^{\dagger}\left(\boldsymbol{x};\omega_j\right)\left[\frac{\partial\mathrm{g}_{\mathrm{MHD}}\left(\boldsymbol{x},\boldsymbol{x}',\omega_j\right)}{\partial\omega}\left(\frac{\partial\delta\boldsymbol{E}\left(\boldsymbol{x}',t\right)}{\partial\mathrm{t}}+i\omega_j\delta\boldsymbol{E}\left(\boldsymbol{x}',t\right)\right)\right]=-i\int d\boldsymbol{x}\;\boldsymbol{e}^{\dagger}\left(\boldsymbol{x};\omega_j\right)\delta\boldsymbol{J}_{\boldsymbol{fast}}\left(\boldsymbol{x},\mathrm{t}\right)\tag{19}$$

The lowest order unknown real field may be written as a sum of eigenmodes $\delta\mathrm{E}\left(\boldsymbol{x}',t\right)=Re\left\{\sum A\left(t;\omega_k\right)e^{-i\omega_k t}\boldsymbol{e}\left(\boldsymbol{x}';\omega_k\right)\right\}$. The real field is therefore half the sum of complex contributions from positive and negative frequencies $\pm\omega_k$. Crucially, the perturbative expansion is only valid in the neighbourhood $\omega\approx\omega_j$. This is a further limitation of the perturbative approach in that eigenmodes must have distinct frequencies, with no 'chirping' sufficiently far as to overlap with any other modes.

The evolution equation for $A\left(t;\omega_j\right)$ is obtained by looking in the neighbourhood of $\omega\approx+\omega_j$

$$\dot{A}\left(t;\omega_j\right)\int d\boldsymbol{x}\int d\boldsymbol{x}'\;\boldsymbol{e}^{\dagger}\left(\boldsymbol{x};\omega_j\right)i\frac{\partial\mathrm{g}_{\mathrm{MHD}}\left(\boldsymbol{x},\boldsymbol{x}',\omega_j\right)}{\partial\omega}\boldsymbol{e}\left(\boldsymbol{x}';\omega_j\right)=2\int d\boldsymbol{x}\;\boldsymbol{e}^{\boldsymbol{i}\omega_j\mathrm{t}}\boldsymbol{e}^{\dagger}\left(\boldsymbol{x};\omega_j\right)\delta\boldsymbol{J}_{\boldsymbol{fast}}\left(\boldsymbol{x},\mathrm{t}\right)\tag{20}$$

with the equivalent redundant expression for $A^{*}\left(t;\omega_j\right)$ obtained for $\omega\approx-\omega_j$

Using the mode energy density averaged over a wave period (cf. Shafranov [17], equation 15.16)

$$\delta W_{MHD}=\int d\boldsymbol{x}\int d\boldsymbol{x}'\;\boldsymbol{e}^{\dagger}(\boldsymbol{x},\omega)\frac{\partial\left(\omega^2K_{MHD}\left(\boldsymbol{x},\boldsymbol{x}',\omega\right)\right)}{\omega\partial\omega}\frac{\epsilon_0}{4}\boldsymbol{e}\left(\boldsymbol{x}',\omega\right)\tag{21}$$

we find for $\mathrm{g}_{\mathrm{MHD}}$

$$\dot{A}\left(t;\omega_j\right)=-\frac{1}{2\delta W_{MHD}}\boldsymbol{e}^{\boldsymbol{i}\omega_j\mathrm{t}}\int d\boldsymbol{x}\;\boldsymbol{e}^{\dagger}\left(\boldsymbol{x};\omega_j\right)\delta\boldsymbol{J}_{\boldsymbol{fast}}\left(\boldsymbol{x},\mathrm{t}\right)\tag{22}$$

$$\delta W_{MHD}=-\frac{i}{4}\int d\boldsymbol{x}d\boldsymbol{x}'\boldsymbol{e}^{\dagger}\left(\boldsymbol{x};\omega_j\right)\frac{\partial\mathrm{g}_{\mathrm{MHD}}\left(\boldsymbol{x},\boldsymbol{x}',\omega_j\right)}{\partial\omega}\boldsymbol{e}\left(\boldsymbol{x}';\omega_j\right)\tag{23}$$

$$\delta\boldsymbol{E}\left(\boldsymbol{x},t;\omega_j\right)=Re\left\{A\left(t;\omega_j\right)\boldsymbol{e}\left(\boldsymbol{x};\omega_j\right)e^{-i\omega_j t}\right\}\tag{24}$$

The linear growth of the real wave amplitude $a\left(t\right)$ may be related with the instantaneous real power transfer to the particles

$$\mathrm{A}\left(t;\omega_j\right)\equiv a_j\left(t\right)e^{\phi_j t},\;\frac{\dot{a}}{a}=\gamma_L+\gamma_{NL}\left(t\right)\tag{25}$$

$$P\equiv\int d\boldsymbol{x}\;\delta\boldsymbol{E}\cdot\delta\boldsymbol{J}_{\boldsymbol{fast}}\tag{26}$$

giving the well-known linear relationship when $\gamma_{NL}\left(t\right)=0$

$$\gamma_L=-\frac{P}{a^2 2\delta W_{MHD}}\tag{27}$$

The solution of the wave-particle problem is thus reduced to choosing the most relevant eigenmodes of the bulk plasma $\boldsymbol{e}\left(\boldsymbol{x};\omega_j\right)$, computing the motion of the resonant particle population $\delta\boldsymbol{J}_{\boldsymbol{fast}}\left(\boldsymbol{x},\mathrm{t}\right)$ in the presence of those eigenmodes, and evolving the amplitude and phase of those modes $A\left(t;\omega_j\right)$ in response to the normalized complex power transfer $\int d\boldsymbol{r}\,\boldsymbol{e}^{\boldsymbol{i}\omega_j\mathrm{t}}\boldsymbol{e}^{\dagger}\left(\boldsymbol{x};\omega_j\right)\delta\boldsymbol{J}_{\boldsymbol{fast}}\left(\boldsymbol{x},\mathrm{t}\right)$ in inverse proportion to the mode energy δW_{MHD}.

2.2. Mode energy for TAE problems

For a cold plasma in the MHD ordering, the linear shear Alfvén response manifests as a polarization drift of ions on an equilibrium magnetic field and $E_{\parallel}=0$

$$\boldsymbol{v}_{\boldsymbol{p}}\left(\boldsymbol{x},t\right)=\frac{d}{dt}\left(\frac{\boldsymbol{E}_{\perp}\left(\boldsymbol{x},t\right)}{\boldsymbol{B}\left(\boldsymbol{x}\right)\Omega_c\left(\boldsymbol{x}\right)}\right)=\frac{m_i}{Ze\boldsymbol{B}^{\boldsymbol{2}}\left(\boldsymbol{x}\right)}\frac{d\boldsymbol{E}_{\perp}\left(\boldsymbol{x},t\right)}{dt}\tag{28}$$

Staying within the linear approximation, we use the equilibrium density

$$n_i(\boldsymbol{x})\boldsymbol{v}_{\boldsymbol{p}}\left(\boldsymbol{x},t\right)=\frac{n_i\left(\boldsymbol{x}\right)m_i}{Ze\boldsymbol{B}^{\boldsymbol{2}}\left(\boldsymbol{x}\right)}\frac{d\boldsymbol{E}_{\perp}\left(\boldsymbol{x},t\right)}{dt}\tag{29}$$

Fourier transforming and identifying the Alfvén speed $v_A=\frac{B}{\sqrt{\mu_0 m_i n_i}}$, we obtain the appropriate generalized Ohm's law for the TAE

$$\tilde{\mathbf{J}}_{\boldsymbol{TAE}}\left(\boldsymbol{x},\omega\right)=\int d\boldsymbol{x}'\left(-i\omega\frac{1}{\mu_0}\delta\left(\boldsymbol{x}'-\boldsymbol{x}\right)\frac{1}{v_A^2\left(\boldsymbol{x}'\right)}\tilde{\mathbf{E}}_{\perp}\left(\boldsymbol{x}',\omega\right)\right)\tag{30}$$

$$\sigma_{TAE}\left(\boldsymbol{x},\boldsymbol{x}',\omega\right)=-i\omega\frac{1}{\mu_0}\delta\left(\boldsymbol{x}'-\boldsymbol{x}\right)\frac{1}{v_A^2\left(\boldsymbol{x}'\right)}\boldsymbol{I}\tag{31}$$

Using the definition of the wave equation

$$\frac{\partial\mathrm{g}_{\mathrm{TAE}}\left(\boldsymbol{x},\boldsymbol{x}',\omega\right)}{\partial\omega}=\frac{2i}{\mu_0}\left(\frac{1}{c^2}+\frac{1}{v_A^2\left(\boldsymbol{x}'\right)}\right)\delta\left(\boldsymbol{x}'-\boldsymbol{x}\right)\tag{32}$$

The first term on the right-hand side of Eq. (32) corresponds to the displacement current which is smaller than the second term by $\frac{v_A^2}{c^2}$ and is neglected. Thus, we obtain the mode energy for the Shear Alfvén wave [19,20]

$$\delta W_{TAE}=\frac{1}{2\mu_0}\int d\boldsymbol{x}\frac{\boldsymbol{e}^{\dagger}\left(\boldsymbol{x};\omega_j\right)\boldsymbol{e}\left(\boldsymbol{x};\omega_j\right)}{v_A^2\left(\boldsymbol{x}\right)}=\frac{1}{\mu_0}\int d\boldsymbol{x}\frac{\overline{\delta\boldsymbol{e}^2}\left(\boldsymbol{x};\omega_j\right)}{v_A^2\left(\boldsymbol{x}\right)}=\frac{1}{\mu_0}\int d\boldsymbol{x}\;\overline{\delta\boldsymbol{b}^2}\left(\boldsymbol{x};\omega_j\right)\tag{33}$$

where we have also included expressions in terms of the real time-averaged square electric $\delta\boldsymbol{e}$ and magnetic $\delta\boldsymbol{b}$ fields of the linear modes for $A\left(t,\omega_j\right)=1$. It should be noted that the eigenmode $\boldsymbol{e}\left(\boldsymbol{x};\omega_j\right)$ must be a clearly distinguishable mode free of any continuum resonance. Where any continuum resonance is present, the resonance region must not be included in computing the mode energy.

2.3. delta-f model for the fast ion current

Solving for the electric field in Maxwell's wave equation requires an evolution equation for the currents in self-consistent response to the field. Most of the current in the perturbative model is due to the linear dielectric currents of the non-resonant oscillatory plasma. For the TAE problem, this Hermitian dielectric current is calculated from the closed linear MHD equations.

The remaining fast current is responsible for resonant drive and damping of the mode. The fast current for an ion of charge Ze is obtained from the distribution function

$$\delta \boldsymbol{J}_{\boldsymbol{i,fast}}(\boldsymbol{x}, t) = \int d\boldsymbol{v}\, f(\boldsymbol{x}, \boldsymbol{v}, t)\, Ze\boldsymbol{v} \tag{34}$$

The motion of the fast particles is assumed to satisfy a Hamiltonian $H(\boldsymbol{x}, \boldsymbol{p}, t)$ with a distribution that evolves according to a collisionless kinetic equation, with no particle sources or sinks. For the full-orbit problem, the Vlasov equation is relevant

$$\frac{\partial f(\boldsymbol{x}, \boldsymbol{v}, t)}{\partial t} + \boldsymbol{v} \cdot \frac{\partial f}{\partial \boldsymbol{x}}(\boldsymbol{x}, \boldsymbol{v}, t) + \frac{Ze}{m}(\boldsymbol{E}(\boldsymbol{x}, t) + \boldsymbol{v} \times \boldsymbol{B}(\boldsymbol{x}, t)) \cdot \frac{\partial f}{\partial \boldsymbol{v}}(\boldsymbol{x}, \boldsymbol{v}, t) = 0 \tag{35}$$

(a general treatment for arbitrary Hamiltonian is left for the Appendix).

In the absence of any perturbation, we assume the existence of an equilibrium

$$\boldsymbol{v} \cdot \frac{\partial F_0}{\partial \boldsymbol{x}}(\boldsymbol{x}, \boldsymbol{v}, t) + \frac{Ze}{m}(\boldsymbol{E_0}(\boldsymbol{x}) + \boldsymbol{v} \times \boldsymbol{B_0}(\boldsymbol{x})) \cdot \frac{\partial F_0}{\partial \boldsymbol{v}}(\boldsymbol{x}, \boldsymbol{v}, t) = 0 \tag{36}$$

Letting $f(\boldsymbol{x}, \boldsymbol{v}, t) = F_0(\boldsymbol{x}, \boldsymbol{v}) + \delta f(\boldsymbol{x}, \boldsymbol{v}, t)$, we seek an evolution equation for the unknown perturbed distribution δf, arriving at

$$\frac{\partial \delta f}{\partial t} + \boldsymbol{v} \cdot \frac{\partial \delta f}{\partial \boldsymbol{x}} + \frac{Ze}{m}(\boldsymbol{E_0} + \boldsymbol{\delta E} + \boldsymbol{v} \times (\boldsymbol{B_0} + \boldsymbol{\delta B})) \frac{\partial \delta f}{\partial \boldsymbol{v}} = -\frac{Ze}{m}(\boldsymbol{v} \times \delta \boldsymbol{B} + \delta \boldsymbol{E}) \frac{\partial F_0}{\partial \boldsymbol{v}} \tag{37}$$

The left-hand side is the time derivative of the perturbed distribution taken along perturbed Hamiltonian trajectories. The right-hand side is the source term that depends only on the perturbed forces and the initial equilibrium. The linear version of the initial value problem is recovered by following unperturbed orbits on the left-hand side of Eq. (37), retaining the perturbations to the motion only in the source term on the right-hand side.

The perturbed forces are calculated from the wave equation forming a closed system of equations for the waves and the perturbed fast current.

2.4. The neutralizing partner electron current

In addition to the bulk plasma currents and the fast ion currents, there are currents associated with the additional neutralizing partner electrons that accompany the fast ions to ensure quasi-neutrality. If those electrons are taken as cold, then only the non-resonant response of the electrons will contribute, and that contribution will be adiabatic changes to the real mode frequency. Taking the electrons as cold will allow separate later inclusion of non-adiabatic thermal Landau electron damping contributions as calculated by other means.

For mode frequencies far below the electron cyclotron frequency, the neutralizing linear electron response is (see Appendix B)

$$\boldsymbol{J}_{\boldsymbol{e,partner}}(\boldsymbol{x}, \omega) = i\omega \frac{Z_{fast}^2 n_{fast} e^2}{m_e \omega^2} E_{\parallel}(\boldsymbol{x}, \omega)\, \hat{\boldsymbol{b}}(\boldsymbol{x}) - Z_{fast} n_{fast} e \frac{\boldsymbol{E}(\boldsymbol{x}, \omega) \times \hat{\boldsymbol{b}}(\boldsymbol{x})}{B_0} \tag{38}$$

Ignoring the parallel electric field for shear Alfvén waves implies the real neutralizing electron current is only due to $E \times B$ motion, which we may write nonlinearly for the real current

$$\delta \boldsymbol{J}_{\boldsymbol{e,partner}}(\boldsymbol{x}, \mathrm{t}) = -Z_{fast} n_{fast} e \frac{\delta \boldsymbol{E}(\boldsymbol{x}, t) \times \boldsymbol{B}(\boldsymbol{x}, t)}{B^2(\boldsymbol{x}, t)} \tag{39}$$

This current must be included in the amplitude evolution equation in order to predict the change in the real mode frequency.

To satisfy the perturbative treatment, this current contribution to the amplitude evolution must be sufficiently small, however this is guaranteed to be cancelled by a component of the fast ion motion which is also $E \times B$ in a magnetized plasma

$$\delta \boldsymbol{J}_{\boldsymbol{i,fast}}(\boldsymbol{x}, t) = e Z_{fast} n_{fast} \left[\frac{\delta \boldsymbol{E}(\boldsymbol{x}, t) \times \boldsymbol{B}(\boldsymbol{x}, t)}{B^2(\boldsymbol{x}, t)} + O\left(\frac{\rho}{L}\right) + \cdots \right] \tag{40}$$

The expression used in HALO is thus $\delta \boldsymbol{J}_{\boldsymbol{fast}}(\boldsymbol{x}, t) = \delta \boldsymbol{J}_{\boldsymbol{i,fast}}(\boldsymbol{x}, t) + \delta \boldsymbol{J}_{\boldsymbol{e,partner}}(\boldsymbol{x}, t)$.

3. Numerical method

3.1. delta-f scheme marker evolution

Using the discrete representation, the ith marker is associated with a unique initial position in phase space (x_i, v_i)

$$\frac{\partial F_0}{\partial \boldsymbol{x}}(\boldsymbol{x}, \boldsymbol{v}, t) \approx \sum_i \delta(\boldsymbol{x} - \boldsymbol{x}(t; \boldsymbol{x_i}, \boldsymbol{v_i}))\, \delta(\boldsymbol{v} - \boldsymbol{v}(t; \boldsymbol{x_i}, \boldsymbol{v_i})) \times \frac{\partial F_0}{\partial \boldsymbol{x}}(\boldsymbol{x}, \boldsymbol{v})\, \Delta^3 x_i \Delta^3 v_i \tag{41}$$

$$\frac{\partial F_0}{\partial \boldsymbol{v}}(\boldsymbol{x}, \boldsymbol{v}, t) \approx \sum_i \delta(\boldsymbol{x} - \boldsymbol{x}(t; \boldsymbol{x_i}, \boldsymbol{v_i}))\, \delta(\boldsymbol{v} - \boldsymbol{v}(t; \boldsymbol{x_i}, \boldsymbol{v_i})) \times \frac{\partial F_0}{\partial \boldsymbol{v}}(\boldsymbol{x}, \boldsymbol{v})\, \Delta^3 x_i \Delta^3 v_i \tag{42}$$

$$\delta f(\boldsymbol{x}, \boldsymbol{v}, t) \equiv \sum_i \delta(\boldsymbol{x} - \boldsymbol{x}(t; \boldsymbol{x_i}, \boldsymbol{v_i}))\, \delta(\boldsymbol{v} - \boldsymbol{v}(t; \boldsymbol{x_i}, \boldsymbol{v_i})) \times \delta f(\boldsymbol{x}, \boldsymbol{v}, t) \Delta^3 x_i \Delta^3 v_i \tag{43}$$

The volume spanned by a marker $\Delta^3 x_i \Delta^3 v_i$ for a uniform and regular loading is defined as the product of lengths taken from halfway between one adjacent marker to another adjacent marker at their initial positions in phase space. The volume is a constant of the motion due to the Hamiltonian nature of the orbits.

Inserting into the delta-f equation and integrating, we find

$$\frac{d}{dt}\delta f_i(t) = -\frac{Ze}{m}(\boldsymbol{v_i}(t) \times \delta \boldsymbol{B}(\boldsymbol{x_i}(t), t) + \delta \boldsymbol{E}(\boldsymbol{x_i}(t), t)) \cdot \left(\frac{\partial F_0}{\partial \boldsymbol{v}}\right)_{\boldsymbol{x}} (\boldsymbol{x_i}(t), \boldsymbol{v_i}(t)) \tag{44}$$

The general form of the 2D equilibrium distribution function assuming no equilibrium electric field is

$$F_0 = \sum_{sgn(v_\parallel)} F(E, \mu, P_\phi; sgn(v_\parallel)) \tag{45}$$

$$n(\boldsymbol{x}) = \sum_{sgn(v_\parallel)} \int d\boldsymbol{v}\, F(E, \mu, P_\phi; sgn(v_\parallel)) \tag{46}$$

where the invariants of motion energy E, gyroinvariant μ and toroidal canonical momentum P_ϕ and $sgn(v_\parallel)$ label each possible equilibrium orbit. The nature of an equilibrium is that it is a function of the unperturbed field and unperturbed particle orbits. Therefore, the coordinate mapping we require is from the space (x, v, t) to the space of invariants of the unperturbed motion.

Perturbed fields do not appear in these equilibrium invariants, it is only the trajectories that are perturbed.

$$F_0 = F\left(E\left(\boldsymbol{x_i}\left(t\right), \boldsymbol{v_i}\left(t\right)\right), \mu\left(\boldsymbol{x_i}\left(t\right), \boldsymbol{v_i}\left(t\right)\right), P_\phi\left(\boldsymbol{x_i}\left(t\right), \boldsymbol{v_i}\left(t\right)\right); sgn(v_\parallel(0))\right) \tag{47}$$

$$P_\phi\left(\boldsymbol{x}, \boldsymbol{v}\right) = mRv_\phi + Ze\psi_0\left(x\right) \tag{48}$$

$$E\left(\boldsymbol{x}, \boldsymbol{v}\right) = \frac{1}{2}mv^2 \tag{49}$$

$$\mu\left(\boldsymbol{x}, \boldsymbol{v}\right) = \frac{\frac{1}{2}mv_\perp^2}{B_0(\boldsymbol{x})} + O\left(\frac{\rho}{L}\right) \tag{50}$$

where we have written only the lowest order in gyroradius expansion $\frac{\rho}{L}$ for the gyroinvariant. Applying the chain rule to the equilibrium equation we arrive at our delta-f scheme in cylindrical coordinates

$$\begin{aligned}\frac{d}{dt}\delta f_i\left(t\right) = &-\delta\dot{v}_R\left[mv_R\left(\frac{\partial F_0}{\partial E}\right)_{\mu,P_\phi} + \frac{\partial\mu}{\partial v_R}\left(\frac{\partial F_0}{\partial\mu}\right)_{E,P_\phi}\right]\\ &-\delta\dot{v}_Z\left[mv_Z\left(\frac{\partial F_0}{\partial E}\right)_{\mu,P_\phi} + \frac{\partial\mu}{\partial v_Z}\left(\frac{\partial F_0}{\partial\mu}\right)_{E,P_\phi}\right]\\ &-\delta\dot{v}_\phi\left[mv_\phi\left(\frac{\partial F_0}{\partial E}\right)_{\mu,P_\phi} + mR\left(\frac{\partial F_0}{\partial P_\phi}\right)_{\mu,E} + \frac{\partial\mu}{\partial v_\phi}\left(\frac{\partial F_0}{\partial\mu}\right)_{E,P_\phi}\right]\end{aligned} \tag{51}$$

with all quantities understood to be measured along a marker trajectory $\left(\boldsymbol{x_i}\left(t\right), \boldsymbol{v_i}\left(t\right)\right)$, and $\delta\dot{\boldsymbol{v}} \equiv \frac{Ze}{m}\left(\boldsymbol{v_i}\left(t\right) \times \delta\boldsymbol{B}\left(\boldsymbol{x_i}\left(t\right), t\right) + \delta\boldsymbol{E}\left(\boldsymbol{x_i}\left(t\right), t\right)\right)$.

When $\frac{\omega}{\Omega} \ll 1$ as expected for low-n shear Alfvén waves, the $\frac{\partial F_0}{\partial\mu}$ contributions to δf may be ignored and we set $\mu\left(t\right) = \mu(0)$. Now we obtain an explicit expression for the work done by the wave on the delta f markers

$$f\left(\boldsymbol{x}, \boldsymbol{v}, t\right) \approx \sum_i \delta\left(\boldsymbol{x} - \boldsymbol{x_i}\left(t\right)\right)\delta\left(\boldsymbol{v} - \boldsymbol{v_i}\left(t\right)\right)\left[F_0\left(\boldsymbol{x}, \boldsymbol{v}\right) + \delta f_i\left(t\right)\right]\Delta^3x_i\Delta^3v_i \tag{52}$$

$$\boldsymbol{J_{i,fast}}\left(\boldsymbol{x}, \mathrm{t}\right) = Ze\sum_i \boldsymbol{v_i}\delta\left(\boldsymbol{x} - \boldsymbol{x_i}\left(t\right)\right)\left[F_0\left(\boldsymbol{x}, \boldsymbol{v_i}\right) + \delta f_i(t)\right]\Delta^3x_i\Delta^3v_i \tag{53}$$

$$\dot{A}_{\boldsymbol{i,fast}}\left(t; \omega_j\right) = -\frac{1}{2\delta W_{TAE}}e^{i\omega_j t}Ze\sum_i \boldsymbol{e}^\dagger\left(\boldsymbol{x_i}(t); \omega_j\right) \cdot \boldsymbol{v_i}\left[F_0\left(\boldsymbol{x_i}\left(t\right), \boldsymbol{v_i}\left(t\right)\right) + \delta f_i\left(t\right)\right]\Delta^3x_i\Delta^3v_i \tag{54}$$

In a 2-D equilibrium, the function $F_0\left(\boldsymbol{x}, \boldsymbol{v}\right)$ is axisymmetric, which implies that we have contributions from the equilibrium proportional to $\int d\phi cosn\phi$ which vanish identically. Dropping the equilibrium contribution therefore reduces the noise significantly, owing to the smallness of δf when compared with F_0

$$\dot{A}_{\boldsymbol{i,fast}}\left(t; \omega_j\right) = -\frac{1}{2\delta W}e^{i\omega_j t}Ze\sum_i \boldsymbol{e}^\dagger\left(\boldsymbol{x_i}(t); \omega_j\right)\boldsymbol{v_i}\delta f_i\left(t\right)\Delta^3x_i\Delta^3v_i \tag{55}$$

As mentioned earlier, correct treatment of the adiabatic contribution to the mode evolution requires the inclusion of the neutralizing partner electrons $\delta\boldsymbol{J_{e,partner}}\left(\boldsymbol{x}, \mathrm{t}\right)$. The natural way to include the neutralizing partner electron contribution in HALO is for each marker to have a correction to its velocity in the complex

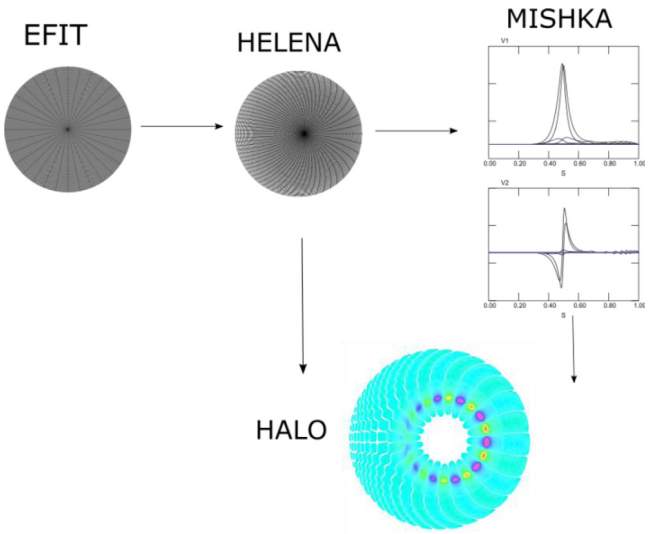

Fig. 1. Alfvénic workflow currently implemented in HALO.

power transfer calculation to remove the $E \times B$ motion giving

$$\dot{A}\left(t; \omega_j\right) = -\frac{1}{2\delta W}e^{i\omega_j t}Ze\sum_i \boldsymbol{e}^\dagger\left(\boldsymbol{x_i}\left(t\right); \omega_j\right)\left(\boldsymbol{v_i} - \boldsymbol{v}_{E\times B}\right) \times \delta f_i\left(t\right)\Delta^3x_i\Delta^3v_i \tag{56}$$

$$\boldsymbol{v}_{E\times B}\left(\boldsymbol{x_i}\left(t\right), t\right) = \frac{\delta\boldsymbol{E}\left(\boldsymbol{x_i}\left(t\right), t\right) \times \boldsymbol{B}\left(\boldsymbol{x_i}\left(t\right), t\right)}{B^2\left(\boldsymbol{x_i}\left(t\right), t\right)} \tag{57}$$

4. Applications

4.1. MHD eigenmodes from MISHKA for TAE studies

The Alfvénic eigenmode workflow currently implemented in HALO is shown schematically in Fig. 1 and is the basis for the examples presented in the rest of this paper. A solution to the Grad–Shafranov equation in cylindrical coordinates is first obtained either via a reconstruction process from experiment via EFIT [21], by prediction, or by postulate. In particular, the profiles $p(\psi)$ and $FF'(\psi)$ and the location of the boundary is required. With the equilibrium profiles and boundary known, a second solution of the Grad–Shafranov equation must be obtained in a straight-field line coordinate system using the HELENA [22] code. This solution produces a high-fidelity equilibrium reconstruction suitable for linear MHD analysis, as well as a coordinate mapping between the cylindrical and straight field line coordinate systems. The high-fidelity equilibrium is provided to the MISHKA [23] linear MHD code and a set of eigenmodes of interest are computed.

The MISHKA eigenmodes are represented with the perturbed fluid velocity in the straight field-line coordinates (s, θ, φ). For ideal modes, MISHKA outputs two variables (v_1, v_2) where v_1 is related to the contravariant radial (s) component of the perturbed flow velocity $\tilde{V}$ and v_2 is related to $\hat{V}^2 = \left[\tilde{V} \times B_0\right]_1$

$$v_1(s, \theta, \varphi) = e^{\lambda t}e^{in\varphi}\sum_m e^{im\theta}\sum_{i=1}^{N}\left(v_{m,i}^1H^1\left(s\right) + dv_{m,i}^1H^2\left(s\right)\right) \tag{58}$$

$$v_2(s, \theta, \varphi) = e^{\lambda t}e^{in\varphi}\sum_m e^{im\theta}\sum_{i=1}^{N}\left(v_{m,i}^2h^1\left(s\right) + dv_{m,i}^2h^2\left(s\right)\right) \tag{59}$$

where the second summation is over radial grid points. The radial dependence is represented using Hermite polynomial basis

Table 1
Parameters chosen for alpha particle driven TAE case.

Parameter	Value
$\epsilon = a/R_0$	0.25
$v_A/2a\Omega_c$	0.03
R_0	3.0 m
B_0	3.0 T
D:T (%)	50:50
q_0	1.82
q_{95}	3.31
T_e	20 keV
T_i	20 keV
$n_\alpha(0)/n_e(0)$	1%

functions of which there are two per radial grid point. For reasons of pollution avoidance v_1 is expressed in terms of cubic Hermite polynomials $H^1(s)$ and $H^2(s)$ whereas v_2 is expressed in terms of quadratic polynomials $h^1(s)$ and $h^2(s)$ [22].

The non-zero covariant components of the vector potential relate to the velocity components and in-turn the electric and magnetic fields in straight-field line coordinates

$$J = \frac{d\psi}{ds}\frac{qR^2}{RB_\phi} \tag{60}$$

$$A_1 = \frac{-iv_2}{\lambda} \tag{61}$$

$$\frac{d\psi}{ds} q\hat{A}_2 = -\frac{v_1}{\lambda} \tag{62}$$

$$\hat{A}_2 \equiv [\boldsymbol{A} \times \boldsymbol{B_0}]^1 / \boldsymbol{B_0^2}. \tag{63}$$

$$J\delta B^1 = -i\left(m\left(\frac{d\psi}{ds}\hat{A}_2\right) + n\left(\frac{d\psi}{ds} q\hat{A}_2\right)\right) \tag{64}$$

$$J\delta B^2 = inA_1 + \frac{\partial}{\partial s}\left(\frac{d\psi}{ds}\hat{A}_2\right) \tag{65}$$

$$J\delta B^3 = \frac{\partial}{\partial s}\left(\frac{d\psi}{ds} q\hat{A}_2\right) - imA_1 \tag{66}$$

$$\delta E_i = -\frac{\lambda A_i}{c} \tag{67}$$

The straight field line representation of the eigenmode is then transformed to conventional cylindrical coordinates using the mapping and metric tensor provided from HELENA. Note that the variables used in MISHKA as repeated above are expressed in cgs Gaussian units, whereas in the rest of the paper we have employed S.I. units.

At time of publication, we did not yet include the adiabatic neutralizing electron contribution, which we expect to be a small correction to the mode frequency.

4.2. Benchmark case: alpha particle driven TAE

For benchmarking and demonstration purposes, an alpha-particle-driven unstable TAE test case was contrived based on a circular equilibrium, with parameters comparable to existing large tokamak experiments (see Table 1).

For simplicity, equilibrium flux functions were polynomials adjusted by hand in HELENA to give a monotonic q-profile with an $n = 6$ TAE found with MISHKA at $s \approx 0.5$, and temperature and density profiles were assumed flat.

Although HALO supports input of arbitrary fast ion distribution functions of the equilibrium form $F(E, \mu, P_\phi; sgn(v_\parallel))$, the alpha particle distribution was taken to be $F = \alpha(E)\,\gamma(P_\phi)$ with polynomial $\gamma(P_\phi) \propto \left(1 - \overline{P_\phi}^2\right)^{10}$ and slowing down distribution [12,24]

$$\alpha(E) \propto \frac{1}{v^3 + v_c^3}\mathrm{Erfc}\left[\frac{E - 3.5\ \mathrm{MeV}}{106 \times 10^3\sqrt{T_i\,[\mathrm{keV}]}}\right]$$

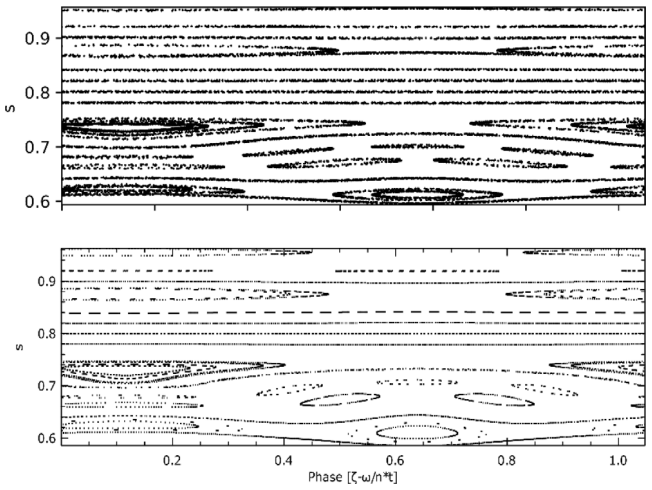

Fig. 2. Comparison of Poincaré plots produced by HALO (top) and HAGIS (bottom). Resonant orbits at critical locations become trapped in the wave forming islands.

$$v_c \equiv \left(3\sqrt{\pi}\frac{m_e Z_1}{4}\right)^{\frac{1}{3}}\sqrt{\frac{2T_e}{m_e}}$$

$$Z_1 = \frac{0.5}{2m_p} + \frac{0.5}{3m_p} \tag{68}$$

4.3. Particle orbit test: wave-particle trapping of resonant orbits comparison with HAGIS

To solve the coupled Maxwell–Vlasov system, the fast particle response to the waves must be faithfully represented. The fields must satisfy Maxwell's equations, and the particles must move according to the Lorentz force law. Equivalently, particles must be shown to move according to the phase-space Lagrangian Equation (D.14).

To test the fast particle response to the eigenmodes, a set of alpha particle markers at different radial locations were launched in the presence of the benchmark $n = 6$ TAE with a fixed mode amplitude $\frac{dB_r}{B_0} = 3 \times 10^{-3}$. All particles were loaded as deeply co-passing $\mu = 0$ and with the same velocity matching the Alfvén speed at the magnetic axis. Both HAGIS and HALO were run recording particle position and wave phase over many orbits, to identify resonantly trapped alpha particle islands in phase space. The comparison of orbits given by the two codes is given in Fig. 2 and shows excellent qualitative agreement.

A more quantitative test comes from conserving the invariant

$$K = E - \frac{\omega}{n}P_\phi \tag{69}$$

This is a particularly stringent test that particles follow orbits derived from the Lagrangian Equation (D.14) because it relates the time and spatial derivatives of the perturbing fields to each other through

$$\frac{d}{dt}E = -\frac{\partial L}{\partial t} \tag{70}$$

$$\frac{d}{dt}P_\phi = \frac{\partial L}{\partial \phi} \tag{71}$$

noting that here, the perturbed field is included in P_ϕ as opposed to the rest of the paper where it denotes the equilibrium invariant $\frac{\partial L_0}{\partial \dot{\phi}}$ (see Appendix). The radial excursions shown in Fig. 2 imply a corresponding change in toroidal canonical momentum due to a breaking of axisymmetry. Fig. 3 shows that although the mode is varying the test particle canonical momentum by up to 10%, the invariant is found to be conserved to better than $\frac{\Delta K}{K} \sim 1 \times 10^{-5}$.

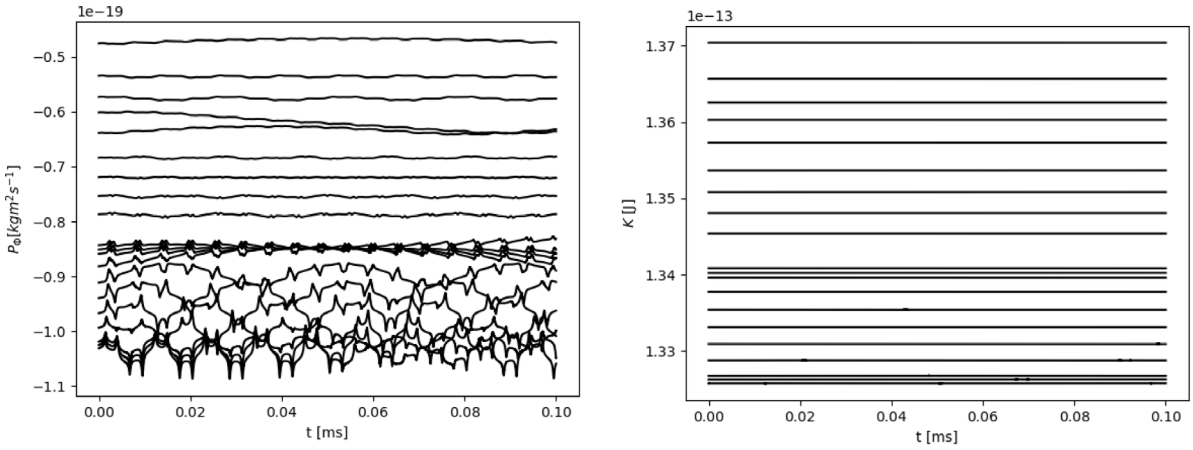

Fig. 3. Variation in toroidal canonical momentum for test particle orbits (left) and the preservation of wave invariant K (right).

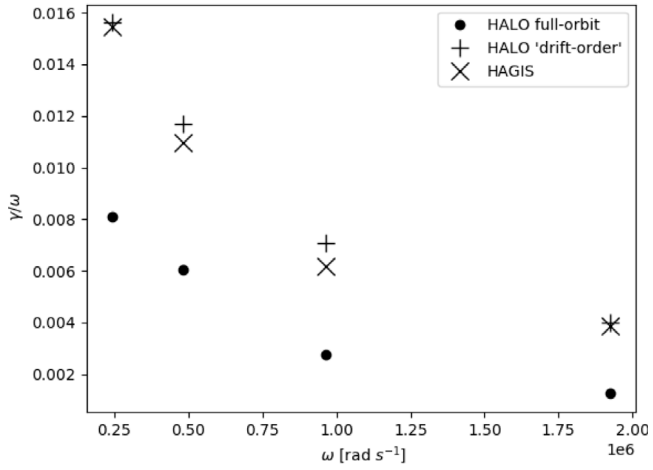

Fig. 4. Comparison of linear growth rates between HAGIS and HALO, varying the mode frequency.

4.4. Stability test: linear growth-rate comparison with HAGIS

Spatial gradients in the particle distributions are a source of free energy for TAEs that propagate in the fast ion-diamagnetic direction due to a universal instability drive [25], with drive occurring if

$$\omega < n\omega_* = n\frac{\partial F/\partial P_\phi}{\partial F/\partial E} \tag{72}$$

The temporal evolution of the TAE is characterized initially by a linear phase where the mode is governed by exponential growth. In this phase, the mode energy is small when compared with the free energy in the gradients. Moreover, the fields of the mode are sufficiently small as to not significantly perturb the equilibrium orbits of the resonant particles.

A scan of frequency for the TAE benchmark case was run in both the HALO and HAGIS codes, and a comparison of the measured linear growth rates is shown in Fig. 4. The linear growth rates in HALO show roughly a factor 2 reduction in drive compared with the HAGIS drift calculation. The difference in drive between HAGIS and HALO lies in the drift approximation for the power transfer evaluating the electric field at the average guiding centre rather than the rapidly varying instantaneous particle location

$$\dot{A}_{\boldsymbol{HAGIS}}\left(t;\omega_j\right) = -\frac{1}{2\delta W}e^{i\omega_j t}Ze\sum_i \boldsymbol{e}^\dagger\left(\boldsymbol{X_i}\left(t\right);\omega_j\right)\boldsymbol{V}_i\delta f_i\left(t\right)\Delta^3 x_i\Delta^3 v_i$$

$$\boldsymbol{x} \equiv \boldsymbol{X} + \boldsymbol{\rho}$$
$$\boldsymbol{V} \equiv \dot{\boldsymbol{X}} \tag{73}$$

The drift-kinetic, gyrokinetic [26,27] and quasi-linear [28] theories can be obtained by gyroaveraging the Vlasov equation over the rapid gyration timescales, resulting in equations in terms of the guiding centre position. Although the guiding centre drift velocity is a good approximation to the average motion of the particles, the field evaluated at the guiding centre is not a good approximation for the average field. At frequencies much lower than the cyclotron frequency, both the gyrokinetic and quasi-linear equations for the perturbed distribution function include terms lacking in the drift theory proportional to $J_0\left(k_\perp\rho\right)$ which captures the finite Larmor radius (FLR) effect of the decreased average electric field experienced by the particle. A simple calculation shows that such a decrease in drive is to be expected for the benchmark case; $k_\perp \approx \frac{m}{r} \approx \frac{12.5}{0.4}$, and at the Alfvén speed $\rho \approx 0.045m$ giving $J_0\left(k_\perp\rho\right) = 0.57$.

For the sole purpose of comparison with the linear HAGIS results, a "drift-order" mode in HALO was implemented, where the electric field in the power transfer Eq. (55) was modified to be evaluated at the guiding centre position

$$\boldsymbol{e}^\dagger\left(\boldsymbol{x_i}\left(\boldsymbol{t}\right);\omega_j\right) \rightarrow \boldsymbol{e}^\dagger\left(\boldsymbol{X_i}\left(t\right);\omega_j\right) \tag{74}$$

giving good agreement in Fig. 4.

Note that before any attempt is made to include this finite Larmor radius correction in a drift-kinetic code such as HAGIS, a technical point worth mentioning here is that the drift velocity $\boldsymbol{V}_i$ in guiding centre codes should be computed to one-higher order in Larmor radius for the resulting power transfer to be consistent with the 1st order drift-kinetic equation, owing to the charge of the particle appearing in the fast particle power transfer $\delta E \cdot \delta j$ [29]. This technical point is the reason for traditional drift-kinetic power calculations being formulated through the pressure rather than the electric field.

4.5. Nonlinear tests: mode saturation and frequency chirping due to phase space holes and clumps

The long-term nonlinear behaviour of the wave-particle system relies on solving the initial value problem for both wave evolution and particle evolution. The verification of linear growth rate implies that the power transfer between waves and particles is correct in the linear phase. We have also shown that test particle orbits are correctly perturbed by a finite mode and are resonantly trapped in the wave.

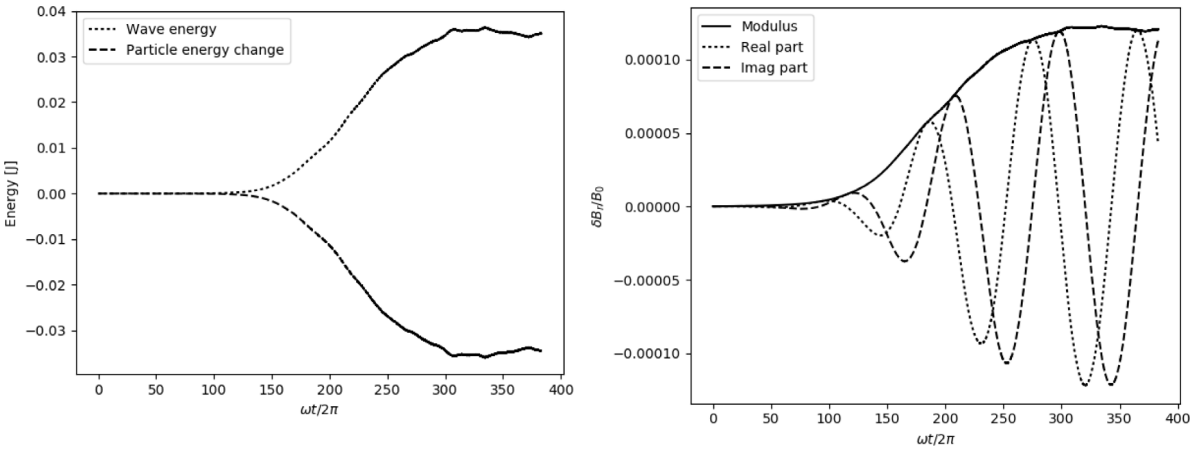

Fig. 5. Nonlinear growth and saturation of the TAE (right), and comparison between change in wave energy and sum of change in particle energy (left).

What remains to be shown is that there is sufficient temporal and spatial resolution in order to faithfully compute the wave power transfer in the nonlinear phase, conserving total energy.

The long-term nonlinear behaviour of the TAE alpha-particle benchmark is given in Fig. 5, showing the classic growth and saturation expected, and the conservation of energy between waves and particles. As the field grows, particle orbits deviate significantly from equilibrium orbits and can become resonantly trapped within the wave potential. The field energy grows as A^2, whereas the region in phase space that can supply energy grows approximately as $A^{3/2}$. When the two energies become comparable, the exponential growth slows until saturation when the gradients in the distribution are removed via phase-mixing of trapped orbits on a timescale comparable with the nonlinear bounce frequency [6].

A further test of nonlinear evolution is the creation of Bernstein–Greene–Kruskal (BGK) nonlinear waves that chirp in frequency. These holes and clumps in phase-space result from the shearing of trapped particle islands as the amplitude of the saturated state is modulated by damping [30,31].

A marginally unstable version of the TAE benchmark was created by considering an additional source current in the wave equation

$$\dot{A}\left(t;\omega_j\right) = -\frac{1}{2\delta W}\boldsymbol{e}^{\boldsymbol{i}\omega_j \mathrm{t}}\int d\boldsymbol{x}\,\boldsymbol{e}^{\dagger}\left(\boldsymbol{x};\omega_j\right)\left[\delta\boldsymbol{J}_{\boldsymbol{fast}}\left(\boldsymbol{x},\mathrm{t}\right)+\delta\boldsymbol{J}_{\boldsymbol{d}}\left(\boldsymbol{x},\mathrm{t}\right)\right] \tag{75}$$

this can be rewritten as an equation for the time varying growth-rate

$$\begin{aligned}\dot{A}\left(t;\omega_j\right) &= \left(\gamma_{\mathrm{fast}}\left(\mathrm{t}\right)-\mathrm{i}\Delta\omega_{fast}\left(t\right)\right)A\left(t;\omega_j\right)\\ &+\left(\gamma_d\left(\mathrm{t}\right)-\mathrm{i}\Delta\omega_d\left(t\right)\right)A\left(t;\omega_j\right)\end{aligned} \tag{76}$$

To produce nonlinear chirping, we assume a linear damping contribution $\gamma_d\left(\mathrm{t}\right)=\gamma_d$, $\Delta\omega_d\left(t\right)=0$

$$\dot{A}\left(t;\omega_j\right) = -\frac{1}{2\delta W}\boldsymbol{e}^{\boldsymbol{i}\omega_j \mathrm{t}}\int d\boldsymbol{x}\,\boldsymbol{e}^{\dagger}\left(\boldsymbol{x};\omega_j\right)\delta\boldsymbol{J}_{\boldsymbol{fast}}\left(\boldsymbol{x},\mathrm{t}\right)+\gamma_d A\left(t;\omega_j\right) \tag{77}$$

The nonlinear TAE benchmark described earlier was repeated with a linear damping term included such that $\frac{\gamma_d}{\gamma_L}=0.9$. Fig. 6 gives the amplitude and frequency evolution of the marginally unstable evolution. The rapid amplitude modulation is typical of marginally stable TAE simulations performed with HAGIS [32] and with other codes [33]. Also evident is the expected steady production of BGK modes sweeping in frequency symmetrically above and below the eigenfrequency as expected from the bump-on-tail theory [34] and observed in previous TAE calculations [35] and has been observed in experiment [36].

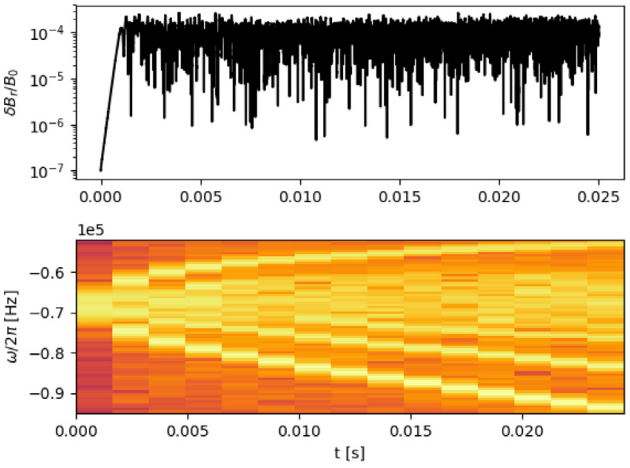

Fig. 6. Amplitude (above) and Fourier spectrogram (below) of the TAE benchmark made marginally unstable.

4.6. Conserved quantities and convergence

The full-orbit motion of δf markers is described by the trajectories obtained from the Lagrangian given by Eq. (D.14) as solved using the orbit-following portions of the LOCUST-GPU code [15] with either of the phase-volume preserving Boris or Strang particle orbit integrators [37].

For fully self-consistent HALO solutions, Eqs. (51) and (55), as well as the particle trajectories specified by Eq. (D.14) are integrated simultaneously in time as an initial value problem. Particles are loaded in 6D phase space using a quasi-random Hammersley sequence [38] in order to reduce noise in the power transfer integral. The rapid variation in the quantity $\boldsymbol{e}^{\dagger}\left(\boldsymbol{x_i}(t);\omega_j\right)\boldsymbol{v}_i$ governs the power transfer timescale, with only the drift contribution having any consequence for Alfvénic modes which oscillate on an $\omega \approx k_{\parallel}v_A$ timescale. Slower still is the growth time of $\dot{A}$ as dictated by the perturbative model. In order to integrate the rapidly varying power transfer between infrequent wave amplitude updates, a 6th order finite difference scheme was used.

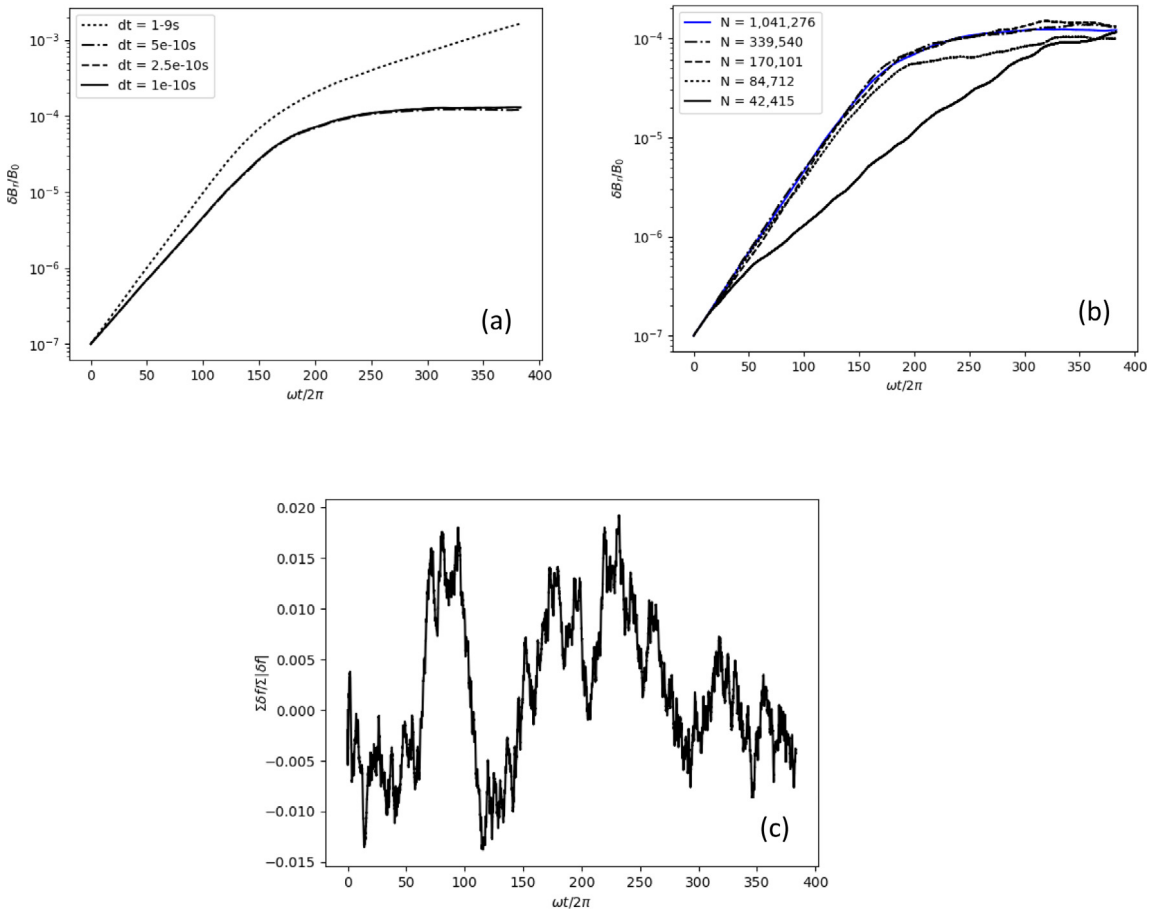

Fig. 7. Convergence properties of the coupled wave-particle system. Plots of convergence with timestep (a) and number of markers (b) are shown, as well as the global conservation of particles in the delta-f scheme (c).

The numerical scheme for coupled wave-particle solution has been tested for convergence in temporal and spatial integration and the results for the benchmark case are given in Fig. 7. A time step of 1×10^{-9} s in the benchmark problem corresponds to $\approx \frac{2\pi}{\Omega_c}\frac{1}{40}$ which is enough to solve the perturbed motion of the particles and conserve orbit invariant K, but appears insufficient in the continual time integration of power transfer $\boldsymbol{e}^{\dagger}\left(\boldsymbol{x_i}(t);\omega_j\right)\boldsymbol{v}_i$. Halving the timestep to $\approx \frac{2\pi}{\Omega_c}\frac{1}{80}$ for the 6th order scheme gives a dramatic improvement, with diminishing returns for further reductions. We have so far only attempted running LOCUST-GPU with simulations below 12 million particles, however we obtain convergence in global energy conservation at around 1 million particles.

Note the complete absence of any slowly growing or slowly decaying amplitude in the converged solution, which has been a stubborn feature in some other delta-f based results but one that we have been able to eliminate with high-order integration and sufficient statistics.

Also related to global energy conservation is the total particle conservation in the delta-f scheme. The perturbed distribution function δf represents the deviation of the distribution function from equilibrium and must therefore contain both positive and negative values as particles are moved from one area of phase space to another. Thus, exact particle number conservation would require that

$$\int d\boldsymbol{x}d\boldsymbol{v}\delta f = \sum \delta f_i \Delta^3 x_i \Delta^3 v_i = 0 \tag{78}$$

The total number of particles in the system includes the unperturbed particles as well as the perturbed particles and the fractional error in the total particle conservation is $\int d\boldsymbol{x}d\boldsymbol{v}\delta f / \int d\boldsymbol{x}d\boldsymbol{v}F_0$, however such a test is rather insensitive by virtue of the small proportion of particles involved in driving the mode, i.e. $\delta f \ll F_0$. A more stringent test $\int d\boldsymbol{x}d\boldsymbol{v}\delta f / \int d\boldsymbol{x}d\boldsymbol{v}|\delta f|$ is presented instead, which is a more direct measure of the error in the code as it computes wave-particle power transfer. The relative conservation of perturbed particles in Fig. 7 implies a random fluctuation in the computed wave growth of the order of 1% with no systematic drift evident.

5. Conclusion and further work

We have presented the theory and validation of a new wave-particle code HALO which perturbatively solves the Maxwell–Vlasov problem when the nonlinearity is dominated by particle currents that do not play a large role in the structure and frequency of the eigenmode. The approach generalizes the HAGIS code by allowing arbitrary particle motion in arbitrary geometry, interacting with eigenmodes whose frequencies are limited only by the particle integration timescale. The workflow currently implemented pertains to the TAE problem in tokamaks, however our presentation has been deliberately general so that this approach can be replicated easily for other kinds of bulk plasma modes.

For our TAE workflow, we have presented benchmarks against the drift-kinetic code HAGIS, with and without the new FLR corrections provided by HALO. The FLR corrections were found to

be significant for an invented benchmark case with parameters that resemble current large tokamak experiments.

We plan to extend HALO to support workflows for modes other than the well-studied TAE problem, such as those located in the ion-cyclotron and ion-acoustic range of frequencies. It is likely that we will use the two-fluid extension to MISHKA, MISHKA3 [39], which includes the Hall-term required in the ion-cyclotron range of frequencies (see Appendix), and for modes at low frequencies, viscous and heat flow effects.

The robustness of this method has undoubtedly been due in part to the Hamiltonian nature of the equations assumed. However it is well understood that the nonlinear evolution of TAEs seen in experiment requires collisions and sources/sinks to be modelled in order to reproduce all of the experimentally observed behaviour, including asymmetric frequency chirping [40]. Collisions have been implemented in various hybrid and gyrokinetic codes [41,42], but a fully consistent delta-f set of equations that includes collisions appears to be far from straightforward. This will likely be the focus of future work to complete the TAE model implemented in HALO.

Acknowledgements

The first author is grateful for the generous hospitality of the Institute for Fusion Studies at the University of Texas Austin which greatly facilitated the development of these ideas. This work has been carried out within the framework of the EUROfusion Consortium and has received funding from the Euratom research and training programme 2014–2018 and 2019–2020 under grant agreement No 633053 for the European Enabling Research Project WP17-ENR-MFE-CCFE-02 and from the RCUK, United Kingdom Energy Programme (Grant Number EP/P012450/1). The views and opinions expressed herein do not necessarily reflect those of the European Commission. To obtain further information on the data and models underlying this paper please contact PublicationsManager@ukaea.uk.

Appendix A. Applicability to the TAE problem versus the EPM problem

TAE stability in a tokamak is a good example of a problem where the orderings used in HALO are valid. The weak currents not captured in the self-adjoint MHD operator include the drive provided by fast particles, the linear damping provided by thermal ions, the linear damping provided by crossing of the continuum, and the nonlinear response. TAEs are discrete modes which exist in gaps in the Shear Alfvén continuum. They are weakly driven and damped and there is good experimental evidence for their mode structure resembling MHD solutions [5].

We turn our attention to the non-resonant nonlinear currents. The fluid current associated with the TAE mode is given by the polarization drift of ions

$$\boldsymbol{v_p}\left(\boldsymbol{x},t\right)=\frac{d}{dt}\left(\frac{\boldsymbol{E}_\perp\left(\boldsymbol{x},t\right)}{\boldsymbol{B}\left(\boldsymbol{x}\right)\Omega_c\left(\boldsymbol{x}\right)}\right)=\frac{m_i}{e_i\boldsymbol{B^2}\left(\boldsymbol{x}\right)}\frac{d\boldsymbol{E}_\perp\left(\boldsymbol{x},t\right)}{dt} \tag{A.1}$$

$$\boldsymbol{v_p}\left(\boldsymbol{x},t\right)=\frac{m_i}{e_i|\boldsymbol{B}+\delta\boldsymbol{B}|^2}\frac{d\boldsymbol{E}_\perp}{dt}\approx\frac{m_i}{e_i\left(B^2+\delta B^2\right)}\frac{d\boldsymbol{E}_\perp}{dt} \tag{A.2}$$

$$\boldsymbol{v_p}\left(\boldsymbol{x},t\right)=\frac{m_i}{e_i}\frac{d\boldsymbol{E}_\perp}{dt}\left(\frac{1}{B^2}-\frac{\delta B^2}{B^4}+\cdots\right) \tag{A.3}$$

The polarization drift is almost completely compressionless, so the polarization current depends on equilibrium ion density

$$\boldsymbol{J_p}\left(\boldsymbol{x},t\right)=n_i\left(\boldsymbol{x}\right)m_i\frac{d\boldsymbol{E}_\perp}{dt}\left(\frac{1}{B^2}-\frac{\delta B^2}{B^4}+\cdots\right) \tag{A.4}$$

Identifying the linear and nonlinear responses

$$\frac{\left|\tilde{\mathbf{J}}_{\boldsymbol{NL}}\right|}{\left|\sigma_{\mathrm{MHD}}\tilde{\mathbf{E}}\right|}=\frac{\delta B^2}{B^2}+\cdots \tag{A.5}$$

A fast particle driven TAE has a linear fast particle driven growth rate $\frac{\gamma}{\omega}\approx$1% with a corresponding saturation amplitude of $\frac{\delta\boldsymbol{B}}{\boldsymbol{B}}\approx 0.1\%$. The perturbative approach which assumes a fixed mode structure is clearly a good approximation in such a regime and the fast particle nonlinearity is the dominant nonlinearity at least until mode saturation.

Conversely, energetic particle modes (EPMs) do not satisfy the perturbative orderings by definition [43,44] and are not valid modes to be considered self-consistently with HALO; specifically, the distribution function in the vicinity of the resonant velocity has strong gradients which produce currents that are responsible both for the drive of the modes as well as the modes' very existence. The coherent motion of the fast current does not merely provide an external drive, but rather, the coherent motion *is* the EPM

$$\frac{\left|\tilde{\mathbf{J}}_{\boldsymbol{NL}}\right|}{\left|\sigma_{\mathrm{MHD}}\tilde{\mathbf{E}}\right|}\sim 1 \tag{A.6}$$

EPMs such as fishbones can also occur at low frequencies where strong damping interactions with the Alfvén continuum produce large response currents

$$\frac{\left|\tilde{\mathbf{J}}_{\bar{\sigma}}\right|}{\left|\sigma_{\mathrm{MHD}}\tilde{\mathbf{E}}\right|}\sim 1 \tag{A.7}$$

The strong continuum damping implies a low-quality linear plasma response at the fishbone frequency. With such a broad bulk plasma response, discussion of a bulk plasma linear "mode" is meaningless.

Appendix B. Mode energy of modes in the ion-cyclotron range

Although this paper has focused on the TAE, HALO is sufficiently general to allow study of arbitrary perturbative eigenmodes. Here we give the derivation of $\frac{\partial g_{COLD}}{\partial\omega}$ required for dW_{COLD} which is valid for any cold plasma eigenmode below the electron cyclotron frequency.

The general cold plasma displacement velocity for a given particle species is [17]

$$\boldsymbol{v}\left(\boldsymbol{x},\omega\right)=i\frac{e}{m}\frac{\omega}{\omega^2-\Omega_{\mathrm{c}}\left(\mathbf{x}\right)^2}\left(\tilde{\mathbf{E}}\left(\boldsymbol{x},\omega\right)-\frac{\Omega_{\mathrm{c}}{}^2\left(\boldsymbol{x}\right)}{\omega^2}\tilde{\mathrm{E}}_{\parallel}\left(\boldsymbol{x},\omega\right)\hat{\boldsymbol{b}}\left(\boldsymbol{x}\right)\right)$$
$$-\frac{\Omega_{\mathrm{c}}(\mathbf{x})^2}{\omega^2-\Omega_{\mathrm{c}}(\mathbf{x})^2}\frac{\tilde{\mathbf{E}}\left(\boldsymbol{x},\omega\right)\times\hat{\boldsymbol{b}}}{B_0} \tag{B.1}$$

Looking first at the electron current, for frequencies well below the electron cyclotron frequency

$$\tilde{\mathbf{J}}_{\boldsymbol{e}}\left(\boldsymbol{x},\omega\right)=i\frac{n_e e^2}{m_e\omega}\tilde{\mathrm{E}}_{\parallel}\left(\boldsymbol{x},\omega\right)\hat{\boldsymbol{b}}\left(\boldsymbol{x}\right)-ne\frac{\tilde{\mathbf{E}}\left(\boldsymbol{x},\omega\right)\times\hat{\boldsymbol{b}}\left(\boldsymbol{x}\right)}{B_0} \tag{B.2}$$

and for ions of charge Ze and cyclotron frequency Ω_{c}

$$\tilde{\mathbf{J}}_{\boldsymbol{i}}\left(\boldsymbol{x},\omega\right)=i\frac{n_i Z^2 e^2}{m_i}\frac{\omega}{\omega^2-\Omega_{\mathrm{c}}\left(\mathbf{x}\right)^2}$$
$$\times\left(\tilde{\mathbf{E}}\left(\boldsymbol{x},\omega\right)-\frac{\Omega_{\mathrm{c}}{}^2\left(\boldsymbol{x}\right)}{\omega^2}\tilde{\mathrm{E}}_{\parallel}\left(\boldsymbol{x},\omega\right)\hat{\boldsymbol{b}}\left(\boldsymbol{x}\right)\right)$$
$$-n_i Ze\frac{\Omega_{\mathrm{c}}(\mathbf{x})^2}{\omega^2-\Omega_{\mathrm{c}}(\mathbf{x})^2}\frac{\tilde{\mathbf{E}}\left(\boldsymbol{x},\omega\right)\times\hat{\boldsymbol{b}}}{B_0} \tag{B.3}$$

Using quasi-neutrality we find, after some manipulation, that the total current is

$$\begin{aligned}\tilde{\mathbf{J}}(\boldsymbol{x},\omega) = &-i\omega\frac{n_i m_i}{B_0^2}\frac{\Omega_c^2}{\Omega_c^2-\omega^2}\tilde{\mathbf{E}}_\perp(\boldsymbol{x},\omega)\\ &+\left(\frac{n_i Z^2 e^2}{m_i\omega}+\frac{ne^2}{m_e\omega}\right)i\tilde{\mathrm{E}}_\parallel(\boldsymbol{x},\omega)\,\hat{\boldsymbol{b}}(\boldsymbol{x})\\ &+\frac{\omega^2}{\Omega_c^2-\omega^2}\frac{ne}{B_0}\tilde{\mathbf{E}}_\perp(\boldsymbol{x},\omega)\times\hat{\boldsymbol{b}}(\boldsymbol{x})\end{aligned} \tag{B.4}$$

We can clearly identify a binormal Hall current which is out of phase with the polarization current. This Hall current is the additional physics required in dW_{COLD} that is ignored for Alfvénic modes. Decomposing the electric field along the orthogonal directions $\hat{e}_1$, $\hat{e}_2$, $\hat{b}$ we obtain the conductivity tensor $\sigma\left(\boldsymbol{x},\boldsymbol{x}',\omega\right)$ (cf. Shafranov [17]) defined through the generalized Ohm's law expression

$$\tilde{\mathbf{J}}(\boldsymbol{x},\omega) = \int\sigma\left(\boldsymbol{x},\boldsymbol{x}',\omega\right)\begin{pmatrix}\tilde{\mathrm{E}}_1\\ \tilde{\mathrm{E}}_2\\ \tilde{\mathrm{E}}_\parallel\end{pmatrix}d^3\boldsymbol{x}' \tag{B.5}$$

$$\sigma_{COLD}(\boldsymbol{x},\boldsymbol{x}',\omega) = \delta(\boldsymbol{x}-\boldsymbol{x}')\begin{pmatrix}A(\boldsymbol{x},\omega) & iH(\boldsymbol{x},\omega) & 0\\ -iH(\boldsymbol{x},\omega) & A(\boldsymbol{x},\omega) & 0\\ 0 & 0 & P(\boldsymbol{x},\omega)\end{pmatrix} \tag{B.6}$$

where

$$A(\boldsymbol{x},\omega) = -i\omega\frac{n_i m_i}{B_0^2}\frac{\Omega_c^2}{\Omega_c^2-\omega^2} \tag{B.7}$$

$$iH(\boldsymbol{x},\omega) = \frac{\omega^2}{\Omega_c^2-\omega^2}\frac{ne}{B_0} \tag{B.8}$$

$$P(\boldsymbol{x},\omega) = i\left(\frac{n_i Z^2 e^2}{m_i\omega}+\frac{ne^2}{m_e\omega}\right) \tag{B.9}$$

Taking the derivative of Eq. (B.6) gives the equation given in Box I.

In the MHD limit $\omega \ll \Omega_c$, the off-diagonal Hall $H(\boldsymbol{x},\omega)$ contributions to the mode energy vanish leaving only the diagonal polarization drift found in Eq. (33) for the perpendicular field.

Appendix C. The adiabatic contribution and the HAGIS and FAC expressions

In HALO, the perturbed distribution in Eq. (55) contains both the real and imaginary components of the correction to frequency. The linear real contribution to the frequency from the imaginary power transfer is also known as the "fluid", "incompressible" or "adiabatic" part of δf [25]

$$\frac{d}{dt}\delta f_{adiabatic}(t) = \frac{d\delta P_\phi}{dt}\frac{\partial F}{\partial P_\phi}+e\frac{d\delta\Phi}{dt}\frac{\partial F}{\partial E}-\frac{d}{dt}\left(\mu\frac{\delta B}{B}\right)\frac{\partial F}{\partial\mu} \tag{C.1}$$

$$\frac{d}{dt}\delta f(t) = \frac{d}{dt}\delta f_{adiabatic}(t)+\frac{d}{dt}h(t) \tag{C.2}$$

where $h(t)$ is the usual label for the non-adiabatic contribution.

Both the HAGIS and FAC codes (as well as the linear CASTOR-K code [45]) explicitly ignore adiabatic contributions to the mode frequency and focus instead on computing the growth rate due to real power transfer. By using MHD for the mode structure, this implies that these codes are ignoring the fast particle pressure contributions to the mode structure and frequency. More recently, there has been work in combining the LIGKA code with HAGIS to weaken this assumption both linearly and non-linearly [46].

We can re-obtain the non-adiabatic HAGIS/FAC evolution equations Eq. 21 in [13] and Eq. 29 in [12] by considering a low-β MHD approximation for an Alfvén eigenmode

$$\nabla\times\sum_m\alpha_m\boldsymbol{B_0} = \delta\boldsymbol{B} \tag{C.3}$$

$$\alpha_m = \frac{k_{\parallel m}\Phi_{\mathrm{m}}}{B_0\omega} \tag{C.4}$$

The power transfer term in Eq. (55) is then proportional to

$$\begin{aligned}e^{i\omega_j t}\boldsymbol{e}^\dagger\left(\boldsymbol{x_i}(t);\omega_j\right)\boldsymbol{v} &= -\sum_m\left(\boldsymbol{v}\cdot\nabla\Phi_{\mathrm{m}}^* e^{i\omega_j t}+\boldsymbol{v}\cdot\frac{\partial}{\partial t}\alpha_m^* e^{i\omega_j t}\boldsymbol{B_0}\right)\\ &= -e^{i\omega_j t}\sum_m\left(\boldsymbol{v}\cdot\nabla\Phi_{\mathrm{m}}^*+i\omega v_\parallel\frac{k_{\parallel m}\Phi_{\mathrm{m}}^*}{B_0\omega}\boldsymbol{B_0}\right)\end{aligned} \tag{C.5}$$

Ignoring the adiabatic contribution implies

$$\frac{d\Phi_{\mathrm{m}}^*}{dt} = \frac{\partial\Phi_{\mathrm{m}}^*}{\partial t}+\boldsymbol{v}\cdot\nabla\Phi_{\mathrm{m}}^* = 0 \tag{C.6}$$

Giving the HAGIS/FAC results

$$A\left(t;\omega_j\right) \equiv X\left(t;\omega_j\right)-iY\left(t;\omega_j\right) \tag{C.7}$$

$$S_{kjm} = \Im m\left\{e^{i(k_m\cdot x_k-\omega_j t)}\Phi_{\mathrm{m}}\right\} \tag{C.8}$$

$$C_{kjm} \equiv \Re e\left\{e^{i(k_m\cdot x_k-\omega_j t)}\Phi_{\mathrm{m}}\right\} \tag{C.9}$$

$$\begin{aligned}\dot{X}\left(t;\omega_j\right) = &\frac{1}{2\delta W}Ze\sum_m\sum_k\left(k_{\parallel m}\left(\boldsymbol{x}_k(t)\right)v_{\parallel k}(t)-\omega_j\right)\\ &\times S_{kjm}\delta f_k(t)\,\Delta^3 x_k\Delta^3 v_k\end{aligned} \tag{C.10}$$

$$\begin{aligned}\dot{Y}\left(t;\omega_j\right) = &-\frac{1}{2\delta W}Ze\sum_m\sum_k\left(k_{\parallel m}\left(\boldsymbol{x}_k(t)\right)v_{\parallel k}(t)-\omega_j\right)\\ &\times C_{kjm}\delta f_k(t)\,\Delta^3 x_k\Delta^3 v_k\end{aligned} \tag{C.11}$$

Appendix D. Two approaches to delta-f — canonical versus non-canonical

A similar delta-f scheme can be constructed for any Hamiltonian motion, where the fast current is given by a density in Hamiltonian phase space $\hat{f}(\boldsymbol{q},\boldsymbol{p},t)$

$$\delta\boldsymbol{J_{i,fast}}(\boldsymbol{q},t) = Ze\int d\boldsymbol{p}\,\hat{f}(\boldsymbol{q},\boldsymbol{p},t)\,\boldsymbol{v}(\boldsymbol{q},\boldsymbol{p},t) \tag{D.1}$$

For any coordinate system the conservation of particles gives

$$\frac{\partial\hat{f}(\boldsymbol{q},\boldsymbol{p},t)}{\partial t}+\frac{\partial}{\partial\boldsymbol{q}}\cdot\left(\dot{\boldsymbol{q}}\hat{f}(\boldsymbol{x},\boldsymbol{p},t)\right)+\frac{\partial}{\partial\boldsymbol{p}}\cdot\left(\dot{\boldsymbol{p}}\hat{f}(\boldsymbol{x},\boldsymbol{p},t)\right) \tag{D.2}$$

The additional assumption of Hamiltonian motion

$$\dot{\boldsymbol{q}} = \frac{\partial H(\boldsymbol{q},\boldsymbol{p},t)}{\partial\boldsymbol{p}},\dot{\boldsymbol{p}} = -\frac{\partial H(\boldsymbol{q},\boldsymbol{p},t)}{\partial\boldsymbol{q}} \tag{D.3}$$

allows the conservation law to be written as a total derivative along the particle orbits

$$\frac{d\hat{f}(\boldsymbol{q},\boldsymbol{p},t)}{dt} = \frac{\partial\hat{f}(\boldsymbol{q},\boldsymbol{p},t)}{\partial t}+\dot{\boldsymbol{q}}\cdot\frac{\partial\hat{f}(\boldsymbol{q},\boldsymbol{p},t)}{\partial\boldsymbol{q}}+\dot{\boldsymbol{p}}\cdot\frac{\partial\hat{f}(\boldsymbol{q},\boldsymbol{p},t)}{\partial\boldsymbol{p}} = 0 \tag{D.4}$$

The distribution function is separated into equilibrium and perturbed portions $\hat{f}(\boldsymbol{q},\boldsymbol{p},t) = \widehat{F_0}(\boldsymbol{q},\boldsymbol{p})+\delta\hat{f}(\boldsymbol{q},\boldsymbol{p},t)$, as is the Hamiltonian $H(\boldsymbol{q},\boldsymbol{p},t) = H_0(\boldsymbol{q},\boldsymbol{p})+\delta H(\boldsymbol{q},\boldsymbol{p},t)$ with the equilibrium satisfying

$$\frac{\partial H_0(\boldsymbol{q},\boldsymbol{p})}{\partial\boldsymbol{p}}\cdot\frac{\partial\widehat{F_0}(\boldsymbol{q},\boldsymbol{p})}{\partial\boldsymbol{q}}-\frac{\partial H_0(\boldsymbol{q},\boldsymbol{p})}{\partial\boldsymbol{q}}\cdot\frac{\partial\widehat{F_0}(\boldsymbol{q},\boldsymbol{p})}{\partial\boldsymbol{p}} = 0 \tag{D.5}$$

$$\frac{\partial \sigma_{COLD}}{\partial \omega}\left(\boldsymbol{x},\boldsymbol{x}',\omega\right) = -\,\delta(\boldsymbol{x}-\boldsymbol{x}')\begin{pmatrix} i\frac{1}{v_A^2}\frac{\Omega_c^2\left(\Omega_c^2+\omega^2\right)}{\left(\Omega_c^2-\omega^2\right)^2} & -\frac{2\Omega_c^2\omega}{\left(\Omega_c^2-\omega^2\right)^2}\frac{ne}{B_0} & 0 \\ \frac{2\Omega_c^2\omega}{\left(\Omega_c^2-\omega^2\right)^2}\frac{ne}{B_0} & i\frac{1}{v_A^2}\frac{\Omega_c^2\left(\Omega_c^2+\omega^2\right)}{\left(\Omega_c^2-\omega^2\right)^2} & 0 \\ 0 & 0 & i\left(\frac{n_i Z^2 e^2}{m_i\omega^2}+\frac{ne^2}{m_e\omega^2}\right)\end{pmatrix} \tag{B.10}$$

Box I.

the evolution of $\delta\hat{f}$ along the particle orbit is then

$$\frac{d}{dt}\delta\hat{f}(\boldsymbol{q},\boldsymbol{p},t) = -\frac{\partial\delta H\left(\boldsymbol{q},\boldsymbol{p},t\right)}{\partial\boldsymbol{p}}\cdot\frac{\partial\widehat{F_0}\left(\boldsymbol{q},\boldsymbol{p}\right)}{\partial\boldsymbol{q}} + \frac{\partial\delta H\left(\boldsymbol{q},\boldsymbol{p}\right)}{\partial\boldsymbol{q}}\cdot\frac{\partial\widehat{F_0}\left(\boldsymbol{q},\boldsymbol{p}\right)}{\partial\boldsymbol{p}} \tag{D.6}$$

An awkward feature of the Hamiltonian approach lies with relating the canonical momentum to measurable quantities i.e.: the velocity. Although the equilibrium $\widehat{F_0}\left(\boldsymbol{q},\boldsymbol{p}\right)$ has no explicit time dependence (by definition), the transformation between $\boldsymbol{p}$ and $\boldsymbol{v}$ is time-dependent because it depends on the perturbation through $\boldsymbol{p}(\boldsymbol{x},\boldsymbol{v},t) = m\boldsymbol{v} + e\boldsymbol{A_0}(\boldsymbol{x}) + e\delta\boldsymbol{A}(\boldsymbol{x},t)$. Choosing to ignore the perturbation in the momentum creates a discrepancy that is linear in the mode amplitude. Given that the growth rate scales as the square root of mode amplitude, an approximation for resonant particles only is $\boldsymbol{p}\left(\boldsymbol{x},\boldsymbol{v},t\right) \approx m\boldsymbol{v} + e\boldsymbol{A_0}(\boldsymbol{x})$ which may be sufficient to capture the non-adiabatic response.

The alternative non-canonical prescription [14] is based on the well-known procedure given by Littlejohn, which starts with the Vlasov equation

$$\delta\boldsymbol{J_{i,fast}}\left(\boldsymbol{x},t\right) = Ze\int d\boldsymbol{v} f\left(\boldsymbol{z},t\right)\boldsymbol{v} \tag{D.7}$$

$$\boldsymbol{z} = (\boldsymbol{x},\boldsymbol{v}) \tag{D.8}$$

$$\frac{\partial f\left(\boldsymbol{z},t\right)}{\partial t} + \dot{\boldsymbol{z}}\cdot\frac{\partial f\left(\boldsymbol{z},t\right)}{\partial\boldsymbol{z}} = 0 \tag{D.9}$$

and relates to any canonical description through a trivial scaling factor $m^3 f\left(\boldsymbol{z},t\right) = \hat{f}\left(\boldsymbol{q},\boldsymbol{p},t\right)$. This is the approach of the existing drift-kinetic and gyrokinetic theory, and the same as used in HALO.

The separation of equilibrium and perturbed motion in phase space is described with a Lagrangian

$$L\left(\boldsymbol{z},\dot{\boldsymbol{z}},t\right) = L_0\left(\boldsymbol{z},\dot{\boldsymbol{z}}\right) + \delta L(\boldsymbol{z},\dot{\boldsymbol{z}},t) \tag{D.10}$$

$$\frac{d}{dt}\frac{\partial L_0\left(\boldsymbol{z},\dot{\boldsymbol{z}}\right)}{\partial\dot{\boldsymbol{z}}} = \frac{\partial L_0\left(\boldsymbol{z},\dot{\boldsymbol{z}}\right)}{\partial\boldsymbol{z}} \rightarrow \dot{\boldsymbol{z}}_{\boldsymbol{0}}(t),$$
$$\frac{d}{dt}\frac{\partial\delta L\left(\boldsymbol{z},\dot{\boldsymbol{z}}\right)}{\partial\dot{\boldsymbol{z}}} = \frac{\partial\delta L\left(\boldsymbol{z},\dot{\boldsymbol{z}}\right)}{\partial\boldsymbol{z}} \rightarrow \delta\dot{\boldsymbol{z}}(t) \tag{D.11}$$

with equilibrium defined through $f\left(\boldsymbol{z},t\right) = F_0\left(\boldsymbol{z}\right) + \delta f(\boldsymbol{z},t)$ and

$$\dot{\boldsymbol{z}}_{\boldsymbol{0}}(t)\cdot\frac{\partial F_0\left(\boldsymbol{z}(t)\right)}{\partial\boldsymbol{z}} = 0 \tag{D.12}$$

and corresponding delta-f equation

$$\frac{d}{dt}\delta f\left(t\right) = -\delta\dot{\boldsymbol{z}}(t)\cdot\frac{\partial F_0\left(\boldsymbol{z}(t)\right)}{\partial\boldsymbol{z}} \tag{D.13}$$

The phase-space Lagrangian in $\boldsymbol{z} = (\boldsymbol{x},\boldsymbol{v})$ is

$$L\left(\boldsymbol{x},\boldsymbol{v},\dot{\boldsymbol{x}},\dot{\boldsymbol{v}},t\right) = \left(m\boldsymbol{v} + e\boldsymbol{A_0} + e\delta\boldsymbol{A}\right)\cdot\dot{\boldsymbol{x}} - \left(e\Phi_0 + e\delta\Phi + \frac{m}{2}\boldsymbol{v}\cdot\boldsymbol{v}\right) \tag{D.14}$$

The transformation of phase-space variables from $\boldsymbol{z} = (\boldsymbol{x},\boldsymbol{v})$ to any other $\boldsymbol{z}$ is completely arbitrary since the Lagrangian is coordinate independent. A particularly simple choice used in the HAGIS/FAC codes is to write the distribution using equilibrium invariants of motion $F = F(E,\mu,P_\phi;\sigma)$. This gives immediately their result when $\dot{\mu}$ is taken as zero and $\boldsymbol{z} = (E,\mu,P_\phi,\ldots)$

$$\frac{d}{dt}E = -\frac{\partial L_0\left(z,\dot{z}\right)}{\partial t} \rightarrow \dot{E} = 0,\ \frac{d}{dt}P_\phi = \frac{\partial L_0\left(z,\dot{z}\right)}{\partial\phi} \rightarrow \dot{P}_\phi = 0 \tag{D.15}$$

$$\frac{d}{dt}\delta f\left(t\right) = -\dot{E}\frac{\partial F_0\left(E,\mu,P_\phi;\sigma\right)}{\partial E} - \dot{P}_\phi\cdot\frac{\partial F_0\left(E,\mu,P_\phi;\sigma\right)}{\partial E} \tag{D.16}$$

References

[1] C. Cheng, M. Chance, Phys. Fluids 29 (1986) 3695.
[2] H.L. Berk, D.N. Borba, B.N. Breizman, S.D. Pinches, S.E. Sharapov, Phys. Rev. Lett. (2001) 87.
[3] L. Chen, Phys. Plasmas 1 (1994) 1519.
[4] Lauber, Phys. Rep. 533 (2013) 33–68.
[5] M.A. Van Zeeland, G.J. Kramer, M.E. Austin, R.L. Boivin, W.W. Heidbrink, M.A. Makowski, G.R. McKee, R. Nazikian, W.M. Solomon, G. Wang, Phys. Rev. Lett. 97 (2006) 135001.
[6] T. O'Neil, Phys. Fluids 8 (1965) 2255.
[7] R.K. Mazitov, Prikl. Mekh. Tekhn. Fiz. 1 (1965) 27–31.
[8] H.L. Berk, B.N. Breizman, Phys. Fluids B 2 (1990) 22–46.
[9] H.L. Berk, B.N. Breizman, M.S. Pekker, Nucl. Fusion 35 (1995) 1713–1720.
[10] R. White, M. Chance, Phys. Fluids 27 (1984) 2455.
[11] Y. Wu, R.B. White, Y. Chen, M.N. Rosenbluth, Phys. Plasmas 2 (1995) 4555.
[12] J. Candy, D. Borba, H.L. Berk, G.T.A. Huysmans, W. Kerner, Phys. Plasmas 4 (1997) 2597.
[13] S.D. Pinches, L.C. Appel, J. Candy, S.E. Sharapov, H.L. Berk, D. Borba, B.N. Breizman, T.C. Hender, K.I. Hopcraft, G.T.A. Huysmans, W. Kerner, Comput. Phys. Commun. 111 (1998) 133–149.
[14] J. Candy, J. Comput. Phys. 129 (1996) 160–169.
[15] R.J. Akers, E. Verwichte, T.J. Martin, S.D. Pinches, R. Lake, 39th EPS Conference & 16th Int. Congress on Plasma Physics, Vol. 12, 2012, pp. 1–4.
[16] D.B. Melrose, Instabilities in Space and Laboratory Plasmas, Cambridge: Cambridge University Press, 1986.
[17] V.D. Shafranov, Electromagnetic Waves in a Plasma Reviews of Plasma Physics, Springer US, Boston, MA, 1967, pp. 1–157.
[18] B.N. Breizman, H.L. Berk, M.S. Pekker, F. Porcelli, G.V. Stupakov, K.L. Wong, Phys. Plasmas 4 (1997) 1559–1568.
[19] B.N. Breizman, S.E. Sharapov, Plasma Phys. Control. Fusion 37 (1995) 1057–1074.
[20] H.L. Berk, B.N. Breizman, H. Ye, Phys. Rev. Lett. 68 (1992) 3563–3566.
[21] L.L. Lao, H.S.t. John, R.D. Stambaugh, A.G. Kellman, W. Pfeiffer, Nucl. Fusion 25 (1985) 1611–1622.
[22] G.T.A. Huysmans, J.P. Goedbloed, W. Kerner, Internat. J. Modern Phys. C 02 (1991) 371–376.
[23] A.B. Mikhailovskii, G.T.A. Huysmans, W.O.K. Kerner, S.E. Sharapov, Plasma Phys. Rep. 23 (1997) 844–857.
[24] J.D. Gaffey, J. Plasma Phys. 16 (149) (1976).
[25] F. Porcelli, R. Stankiewicz, W. Kerner, Phys. Plasmas 1 (1994).
[26] A.N. Simakov, P.J. Catto, Phys. Plasmas 12 (2005) 1–9.
[27] H. Qin, W.M. Tang, G. Rewoldt, Phys. Plasmas 5 (1035) (1998).
[28] C.F. Kennel, F. Engelmann, Phys. Fluids 9 (2377) (1966).
[29] M.N. Rosenbluth, N. Rostoker, Phys. Fluids 2 (1959) 23.

[30] T.H. Dupree, Phys. Fluids 15 (1972) 334.
[31] H.L. Berk, B.N. Breizman, N.V. Petviashvili, Phys. Lett. A 234 (1997) 213–218.
[32] M. Fitzgerald, S.E. Sharapov, P. Rodrigues, D. Borba, Nucl. Fusion 56 (2016) 112010.
[33] H.V. Wong, H.L. Berk, Phys. Plasmas 5 (1998) 2781.
[34] M.K. Lilley, R.M. Nyqvist, Phys. Rev. Lett. 112 (2014) 155002.
[35] S.D. Pinches, H.L. Berk, M.P. Gryaznevich, S.E. Sharapov, J.-E. Contributors, Plasma Phys. Control. Fusion 46 (2004) S47–S57.
[36] M.P. Gryaznevich, S.E. Sharapov, Nucl. Fusion 46 (2006) S942–S950.
[37] G.L. Delzanno, E. Camporeale, J. Comput. Phys. 253 (2013) 259–277.
[38] J.H. Halton, Numer. Math. 2 (1960) 84–90.
[39] A. Mikhailovskii, Plasma Phys. Control. Fusion 40 (1998) 1907.
[40] M.K. Lilley, B.N. Breizman, S.E. Sharapov, Phys. Plasmas 17 (2010).
[41] Y. Todo, H.L. Berk, B.N. Breizman, Nucl. Fusion 52 (2012) 033003.
[42] M.D.J. Cole, A. Biancalani, A. Bottino, R. Kleiber, A. Könies, A. Mishchenko, Phys. Plasmas 24 (2017) 022508.
[43] A. Fasoli, C. Gormenzano, H. Berk, B. Breizman, S. Briguglio, D. Darrow, N. Gorelenkov, W. Heidbrink, A. Jaun, S. Konovalov, R. Nazikian, J.-M. Noterdaeme, S. Sharapov, K. Shinohara, D. Testa, K. Tobita, Y. Todo, G. Vlad, F. Zonca, Nucl. Fusion 47 (2007) S264–S284.
[44] F. Zonca, L. Chen, Phys. Plasmas 21 (2014).
[45] D. Borba, W. Kerner, J. Comput. Phys. 153 (1999) 101–138.
[46] M. Schneller, Transport of Super-Thermal Particles and their Effect on the Stability of Global Modes in Fusion Plasmas, (Ph.D. thesis), Technische Universität München, 2013.